

See discussions, stats, and author profiles for this publication at: <https://www.researchgate.net/publication/292946739>

Hafnium, oxygen, neodymium, strontium, and lead isotopic constraints on magmatic evolution of the supereruptive southern Black Mountains volcanic center, Arizona, U.S.A.: A combine...

Article in American Mineralogist · February 2016

Impact Factor: 1.96 · DOI: 10.2138/am-2016-5127

READS

104

7 authors, including:



Susanne M. McDowell

Hanover College

9 PUBLICATIONS 392 CITATIONS

[SEE PROFILE](#)



Christopher Michael Fisher

University of Alberta

29 PUBLICATIONS 188 CITATIONS

[SEE PROFILE](#)



Calvin F. Miller

Vanderbilt University

158 PUBLICATIONS 5,366 CITATIONS

[SEE PROFILE](#)



Jonathan S. Miller

San Jose State University

84 PUBLICATIONS 1,711 CITATIONS

[SEE PROFILE](#)

SPECIAL COLLECTION: PERSPECTIVES ON ORIGINS AND EVOLUTION OF CRUSTAL MAGMAS

Hafnium, oxygen, neodymium, strontium, and lead isotopic constraints on magmatic evolution of the supereruptive southern Black Mountains volcanic center, Arizona, U.S.A.: A combined LASS zircon–whole-rock study

SUSANNE M. McDOWELL^{1,2,*}, SARAH OVERTON³, CHRISTOPHER M. FISHER⁴, WILLIAM O. FRAZIER¹, CALVIN F. MILLER¹, JONATHAN S. MILLER³, AND RITA C. ECONOMOS^{5,†}

¹Earth and Environmental Sciences, Vanderbilt University, PMB 351805, 2301 Vanderbilt Place, Nashville, Tennessee 37235-1805, U.S.A.

²Department of Geology, Hanover College, 484 Ball Drive, Hanover, Indiana 47243, U.S.A.

³Geology Department, San Jose State University, One Washington Square, San Jose, California 95192, U.S.A.

⁴School of the Environment, Washington State University, P.O. Box 642812, Pullman Washington 99164-2812, U.S.A.

⁵Department of Earth and Space Sciences, University of California–Los Angeles, 595 Charles Young Drive East, P.O. Box 951567, Los Angeles, California 90095, U.S.A.

ABSTRACT

The >700 km³ Peach Spring Tuff (PST), erupted at 18.8 Ma from the Silver Creek caldera in the southern Black Mountains volcanic center (SBMVC) of western Arizona, is the only supereruption-scale ignimbrite in the northern Colorado River Extensional Corridor. The SBMVC contains pre- and post-caldera volcanic rocks and caldera-related intrusions (~19–17 Ma) that provide a detailed petrologic record of ignimbrite antecedence and aftermath.

Whole-rock Sr-Nd-Pb-Hf isotopic data combined with complementary zircon O and Hf isotopic data from a suite of pre- through post-PST samples provide robust constraints on (1) how the SBMVC evolved with respect to magmatic sources and processes throughout its ~2 Ma history and (2) the petrogenetic relationships between the PST and slightly younger intracaldera plutons. Both pre- and post-PST units have isotopic ranges ($\epsilon_{\text{Nd}} = -8.3$ to -11.6 , $\epsilon_{\text{Hf}} = -8.2$ to -14.0 , $^{87}\text{Sr}/^{86}\text{Sr}_i = 0.709$ – 0.712 ; $^{206}\text{Pb}/^{204}\text{Pb} = 18.19$ – 18.49 , $^{207}\text{Pb}/^{204}\text{Pb} = 15.60$ – 15.62 , $^{208}\text{Pb}/^{204}\text{Pb} = 38.95$ – 39.29) that fall within the spectrum of Miocene Colorado River Extensional Corridor rocks and are consistent with mixing of substantial fractions of Proterozoic (Mojave) crust and juvenile material derived from regional enriched mantle. Compared to the PST, which has relatively uniform isotopic ratios ($\epsilon_{\text{Nd}} = -11.4$ to -11.7 , $\epsilon_{\text{Hf}} = -13.8$ to -14.3 , $^{87}\text{Sr}/^{86}\text{Sr}_i = 0.709$ – 0.712 ; $^{206}\text{Pb}/^{204}\text{Pb} = 18.20$ – 18.29 , $^{207}\text{Pb}/^{204}\text{Pb} = 15.60$ – 15.62 , $^{208}\text{Pb}/^{204}\text{Pb} = 39.02$ – 39.33), individual pre- and post-PST units are isotopically more variable and generally more primitive.

Consistent with whole-rock isotopes, zircon ϵ_{Hf} (-8 to -14) and oxygen $\delta^{18}\text{O}$ ($+4.5$ to $+7.2\text{\textperthousand}$) for most pre- and post-PST units also have wider ranges and more mantle-like values than those of the PST (-12 to -15 , $+6.1$ to $+7.1\text{\textperthousand}$). Moreover, zircon isotopic compositions decrease in post-PST samples. A few zircons from post-PST intrusions have $\delta^{18}\text{O}$ values lower than mantle values ($<+5\text{\textperthousand}$), suggesting incorporation of hydrothermally altered rock.

Whole-rock and zircon elemental and isotopic analyses indicate that (1) most pre- and post-PST units are less evolved and less homogenized than the PST itself; (2) intrusions in the Silver Creek caldera are petrogenetically distinct from the PST and therefore represent discrete magmatic pulses, not unerupted PST mush; (3) enriched mantle input increased in the SBMVC following the paroxysmal PST eruption; (4) post-PST history of the SBMVC was characterized by periodic influx of magmas with varying juvenile fractions into pre-existing mushy or solidified intrusions, resulting in variable and incomplete hybridization; and (5) melting and assimilation of hydrothermally altered crust played a relatively minor role in the generation and evolution of magmas in the SBMVC.

Keywords: Volcanic center, petrogenesis, zircon, oxygen isotopes, Sr isotopes, Hf isotopes, Nd isotopes, Pb isotopes, supereruption

INTRODUCTION

The southern Black Mountains volcanic center (SBMVC), located in the northern Colorado River Extensional Corridor

(CREC) of northwestern Arizona, comprises the >700 km³ Peach Spring Tuff (PST); its source, the Silver Creek caldera; and well-exposed pre- to post-PST volcanic units and intracaldera intrusions that were emplaced over a period of 2 m.y. (Ferguson et al. 2013; Pamukcu et al. 2013; McDowell et al. 2014). The completeness of the SBMVC's magmatic record and the recent finding that the age of part of the intracaldera intrusion complex is indistinguishable from that of the PST (McDowell et al. 2014)

* E-mail: mcdowell@hanover.edu

† Current address: Roy M. Huffington Department of Earth Sciences, Southern Methodist University, 3225 Daniel Avenue, Dallas, Texas 75205, U.S.A.

Special collection information can be found at <http://www.minsocam.org/MSA/AmMin/special-collections.html>.

make it an attractive locality for exploring two questions that have attracted widespread interest: (1) How do volcanic centers that produce large-volume explosive eruptions evolve with respect to magmatic source(s), composition, and processes (e.g., Lipman 2007; Tappa et al. 2011; Watts et al. 2011, 2012)? (2) What are the petrogenetic relationships between volcanic rocks and spatially associated subvolcanic intrusions (e.g., Bachmann and Bergantz 2004; Bachmann et al. 2007; Glazner et al. 2008)? More specifically, what are the relationships between very large ignimbrites and the approximately contemporaneous plutons in their source calderas (e.g., Lipman 1984; Bachmann and Bergantz 2008; Zimmerer and McIntosh 2012a, 2012b; Mills and Coleman 2013)? In the case of the SBMVC, are the intracaldera intrusions unerupted remnants of supereruption magmas, or do they represent discrete magmatic pulses?

To address these questions with respect to the SBMVC, we apply a combination of whole-rock Sr-Nd-Hf-Pb and in situ zircon O and Hf isotopic analysis. Because isotopes of Sr, Nd, Pb, and Hf are not appreciably fractionated as a consequence of closed-system processes, their ratios remain effectively constant in the products of closed-system crystallization and melt segregation on the timescales involved. Only open-system events, like magma mixing and crustal assimilation, can create isotopic variability within a magma. Moreover, radiogenic isotopic ratios constrain source composition and age. Previous studies have shown that Proterozoic, Mesozoic, and Miocene-age rocks in the Mojave Desert region, which includes the SBMVC, have distinctive Sr, Nd, and Pb isotopic signatures (e.g., Bennett and DePaolo 1987; Farmer et al. 1989; Wooden and Miller 1990; Feuerbach et al. 1993; Miller and Wooden 1994; Falkner et al. 1995; Metcalf et al. 1995; Miller et al. 2000; Bachl et al. 2001; Erickson et al. 2004). The isotopic characteristics established by these studies serve as regional benchmarks against which we can compare the isotopic compositions of the SBMVC and with which we can constrain sources and open-system processes such as assimilation and magma mixing.

The introduction of high-precision, high-resolution analytical techniques has permitted determination of isotopic ratios in situ in minerals. Hafnium and oxygen isotopic compositions of zircons offer particularly valuable insights into magmatic origins and evolution. More sensitively than whole-rock analyses, in situ Hf isotope data provide constraints on magmatic sources, degree of magmatic heterogeneity, and open-system processes (e.g., Hawkesworth and Kemp 2006; Kemp et al. 2006, 2007, 2010; Drew et al. 2013). Oxygen isotope ratios determined in situ in zircon shed complementary light on magmatic characteristics and processes; in particular, they document varying input from crustal materials that have interacted with surface water (e.g., Bindeman and Valley 2001; Valley et al. 2005; Hawkesworth and Kemp 2006; Bindeman et al. 2007; Kemp et al. 2007; Watts et al. 2011, 2012).

We combine our comprehensive isotopic data with new and existing whole-rock and zircon elemental data to characterize representative volcanic and intrusive units in the SBMVC. We then apply the constraints offered by the data set to investigate magmatic sources and processes and plutonic-volcanic connections.

GEOLOGICAL CONTEXT

The 70 to 100 km wide northern Colorado River Extensional Corridor (CREC) is a zone of north-northwest-trending crustal blocks bounded by normal faults at the eastern edge of the Basin and Range in western Arizona, southern Nevada, and southeastern California (Fig. 1; Faulds et al. 1990, 2001). It formed between ~20 and 12 Ma when lithospheric extension, preceded and accompanied by intermediate to silicic magmatism, dismembered Proterozoic- and Mesozoic-age continental crust (Faulds et al. 1990, 2001; Varga et al. 2004). Evidence for the region's tectonic and volcanic upheaval during the middle Miocene is well preserved within the northern CREC as thick sequences (>3 km) of volcanic and sedimentary strata and dissected coeval plutons (e.g., Faulds et al. 1990; Falkner et al. 1995; Bachl et al. 2001; Miller and Miller 2002; Metcalf 2004; Walker et al. 2007; Lang et al. 2008).

The southern Black Mountains produced the most voluminous eruption in the northern CREC: the "supereruption" of the Peach Spring Tuff (PST) at 18.8 Ma (Lidzbarski et al. 2012; Ferguson et al. 2013; Pamukcu et al. 2013). The PST ignimbrite is widely recognized in southeastern California, southern Nevada, and western Arizona (Young and Brennan 1974; Glazner et al. 1986; Buesch and Valentine 1986) (Fig. 1a). Its source, the Silver Creek caldera, was dismembered during post-PST extension, with a smaller fragmented now exposed across the Colorado River in the Sacramento Mountains, California (Ferguson et al. 2013).

Although the PST represents by far the largest eruption in the southern Black Mountains, it was bracketed by ~2 million years of volcanic activity (Pearthree et al. 2010; McDowell et al. 2012, 2014; Table 1). The Silver Creek caldera and its environs (Fig. 1) provide a temporal record of pre- to post-PST magmatism in the vicinity of the caldera (Lang 2001; Lang et al. 2008; McDowell et al. 2014).

We define the SBMVC to encompass the exposures of igneous rocks that predate and immediately post-date the PST, in the southern Black Mountains where a thick pre-PST volcanic section is exposed (Fig. 1). The northern boundary of the SBMVC is near Union Pass, a zone identified by Murphy and Faulds (2003) and Murphy et al. (2004) as a "temporal domain boundary" between 19–17 Ma extension to the south and <16 Ma extension to the north (Fig. 1); it is also at or near the northernmost extent of thick, intermediate-composition pre-PST volcanic units (Faulds et al. 1995; Lang 2001; Murphy and Faulds 2013). The western boundary is buried beneath Quaternary alluvium that fills the broad basin through which the Colorado River flows; Kingman, Arizona, where pre-PST trachyte is absent from the stratigraphic section, is at the eastern margin. The southern boundary is at the southernmost extent of the Black Mountains, approximately 20 km southeast of the Silver Creek caldera (Fig. 1).

STAGES OF SBMVC MAGMATISM

We divide SBMVC magmatism into three stages based on this and previous studies (e.g., Lang et al. 2008; Pearthree et al. 2010; Pamukcu et al. 2013; McDowell et al. 2014): (1) initial, predominantly intermediate-composition, effusive volcanism; (2) the dominantly silicic PST eruption; and finally (3) compositionally diverse, small-volume volcanism and epizonal intrusions (Fig. 2).

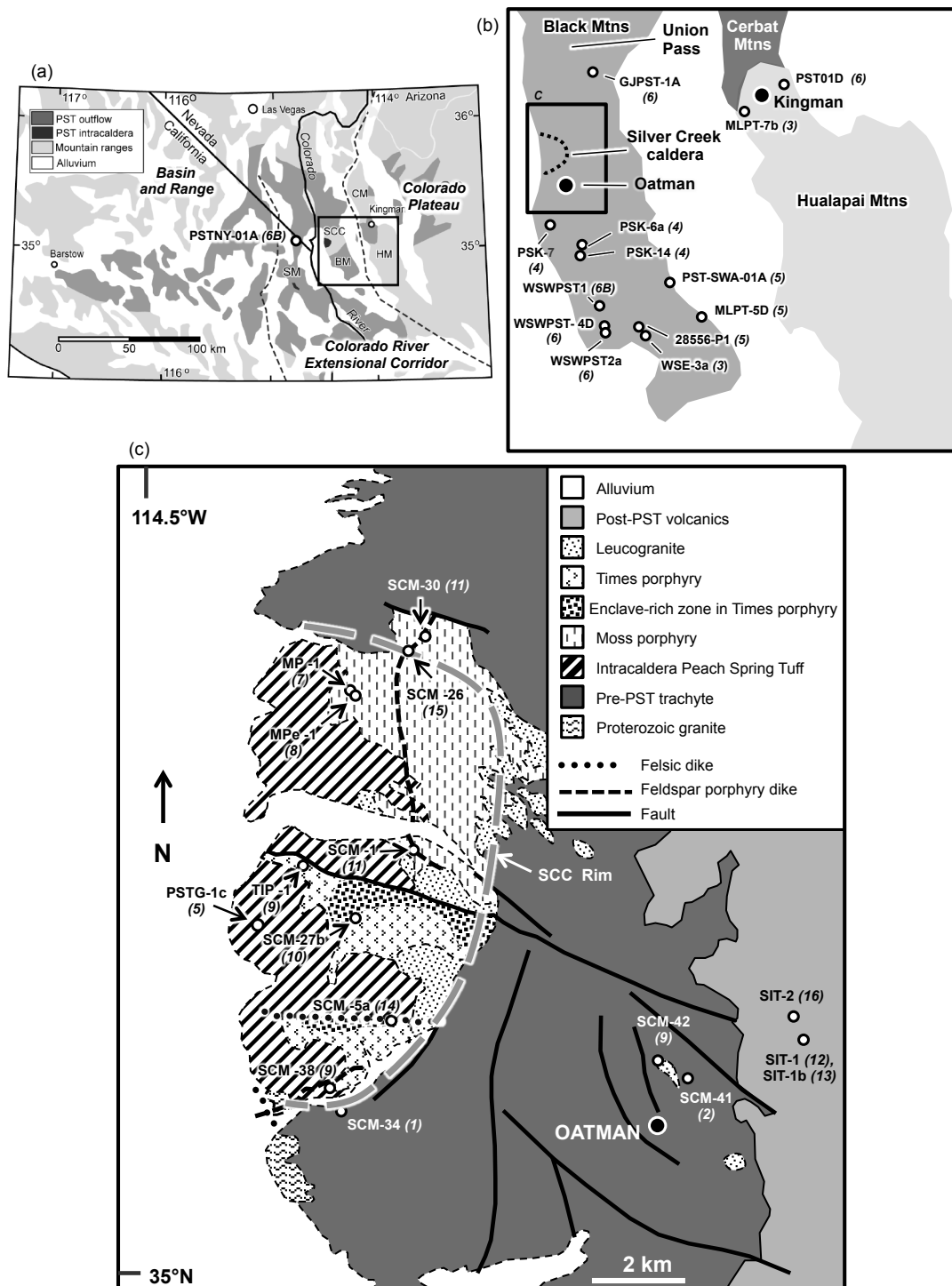


FIGURE 1. (a) Extent of the 18.8 Ma rhyolitic Peach Spring Tuff and location of its source, the Silver Creek Caldera (Ferguson et al. 2013; Pamukcu et al. 2013). BR = Basin and Range, CP = Colorado Plateau, CREC = Colorado River Extensional Corridor, SM = Sacramento Mountains, BM = Black Mountains, CM = Cerbat Mountains, HM = Hualapai Mountains, SCC = Silver Creek Caldera. Box shows approximate extent of the Southern Black Mountains Volcanic Center (SBMVC). (b) Map of SBMVC within area of box shown in a. Sample locations are shown with their unit numbers (*italicized*, following designations in Table 1). Box shows area of c. BM = Black Mountains, CM = Cerbat Mountains, HM = Hualapai Mountains. (c) Geology and sample locations in the Oatman-Silver Creek area, southern Black Mountains. The Silver Creek caldera and its immediate environs includes intracaldera PST, post-PST intrusions, and pre- and post-PST volcanics (geology from Ferguson et al. 2013).

TABLE 1. Stages of SBMVC magmatism and units analyzed

Stage of SBMVC magmatism	Character of magmatism and magmatic products	Unit no.	Unit name	Sample names* (Ages, where available)
Post-PST Volcanics (18.5–16.9 Ma^a)	Compositionally diverse effusive and explosive volcanism	16	Trachyte Lava (Cottonwood)	SIT-2 (17.58 ± 0.05 Ma) ^d
		13	Felsic Lava Enclave	SIT-1b
		12	Felsic Lava	SIT-1 (18.50 ± 0.16 Ma) ^c
Post-PST Intrusions (18.8–18.2 Ma)	Intermediate to silicic intracaldera intrusive magmatism (Times Porphyry, Moss Porphyry); intrusion of compositionally diverse crosscutting dikes within and in the immediate vicinity of the caldera	15	Mafic Dike	SCM-26
		14	Felsic Porphyry Dikes	SCM-5a (18.21 ± 0.07 Ma) ^c , BCD , SCM-42
		11	Feldspar Porphyry Dikes	SCM-1b (18.65 ± 0.07 Ma) ^c , SCM-13 , SCM-30
		10	Times Enclave	SCM-27b
		9	Times Porphyry	TIP-1 (18.63 ± 0.08 Ma) ^c , SCM-37 , SCM-20 , SCM-38
		8	Moss Enclave	MPe1
		7	Moss Porphyry	MP1 (18.76 ± 0.11 Ma) ^c , SCM-6 (18.84 ± 0.15 Ma) ^c
		6B	Enclaves in Outflow	WSWPST1 , PST-NY01A
		6A	Outflow Rhyolite Tuff ^e	WSWPST-4D , GJPST-1A , WSWPST-2a , PST01D
PST (18.8 Ma)^{a,b}	PST supereruption, producing phenocryst-rich trachytic intracaldera and proximal outflow tuff and rhyolitic outflow tuff (>700 km ³ ; covers ~32,000 km ²)	5	Intacaldera and Outflow Phenocryst-rich Trachyte Tuff ^e	PST-SWA-01A , PSTG-1c , MLPT-5D , 28556-P1
		4	Trachyte and Trachyandesite Lavas	PSK-6a , PSK-7 , PSK-14 , PST-11
Pre-PST Volcanics (~19–18.8 Ma)	Thick (up to ~1 km), phenocryst-rich intermediate-composition trachytic effusive magmatism (~10 ³ km ³); intermediate composition explosive volcanism (Cook Canyon Tuff); minor intermediate-composition effusive magmatism	3	Cook Canyon Tuff	WSE-3a , MLPT-7a , MLPT-7b
		2	Gold Road Trachyte ^f	SCM-41
		1	Alcyone Trachyte ^f	SCM-34 (19.01 ± 0.26 Ma) ^c

Notes: a = Ferguson et al. 2013 (sanidine Ar/Ar). b = Lidzbarski et al. 2012 (TIMS and SHRIMP zircon U-Pb). c = McDowell et al. 2014 (TIMS zircon U-Pb). d = McIntosh and Ferguson, unpublished data (sanidine Ar/Ar). e = Frazier 2013. f = Ransome 1923; Thorson 1971. g = Lang 2001; Lang et al. 2008.

* Samples in **bold**: whole-rock isotopic analysis; samples in *italics*: zircon isotopic analysis. Samples in **bold** and *italic*: whole-rock and zircon isotopic analyses.

(1) Pre-PST magmatism is dominated by thick, phenocryst-rich (~10–40%, biotite and plagioclase) trachytic, trachydacitic, and trachyandesitic lavas that overlie Precambrian basement and are exposed from Union Pass to the southernmost Black Mountains (Fig. 1; Ransome 1923; Thorson 1971; DeWitt et al. 1986; Faulds et al. 1999; Lang 2001; Murphy 2004; Lang et al. 2008; Pearthree et al. 2010). These intermediate-composition lavas exceed ~1 km thickness throughout the southern 40 km of the Black Mountains. Approximately 15 km north of Silver Creek caldera (Fig. 1), the same lavas thin to less than 200 m (Lang et al. 2008; Ferguson et al. 2013; Murphy 2004; Murphy et al. 2013). This suggests a total volume on the order of 10³ km³. Faulds et al. (1999) obtained biotite ⁴⁰Ar/³⁹Ar ages for pre-PST lava of 19.19 ± 0.06 and 19.59 ± 0.03 Ma. CA-TIMS U-Pb dating of zircons extracted from Alcyone trachyte yielded a weighted mean age of 19.01 ± 0.2 Ma (McDowell et al. 2014). The Alcyone trachyte comprises a thick sequence of lavas at the base of the pre-PST section (Ransome 1927; Thorson 1971; DeWitt et al. 1986). Units higher in the section include the Gold Road trachyte (Ransome 1927; Thorson 1971; DeWitt et al. 1986); thinner mafic to intermediate lavas including the Wrigley Mine basaltic trachyandesite and Esperanza trachyte (Pearthree et al. 2010), exposed to the southeast of the Silver Creek caldera and near Union Pass (Fig. 1; Pearthree et al. 2010; Ferguson et al. 2013; Murphy et al. 2013); and the Cook Canyon Tuff, an ignimbrite ranging from ~10–100 m in thickness that was produced by the largest explosive eruption in the SBMVC other than the PST (Buesch and Valentine 1986; Murphy 2004; Murphy et al. 2013).

(2) The PST consists of a >0.5 km thick, phenocryst-rich intracaldera trachyte that fills Silver Creek caldera, and outflow that includes trachyte at the tops of some proximal exposures but is dominated by high-silica rhyolite (Pamukcu et al. 2013; Ferguson et al. 2013; Frazier 2013). Outflow PST is exposed over

an area of 32 000 km² (Fig. 1; Buesch 1991; Ferguson et al. 2013).

⁴⁰Ar/³⁹Ar dating of PST sanidine yielded an age of 18.78 ± 0.02 Ma (Ferguson et al. 2013); a correction of systematic bias using the algorithms of Renne et al. (2010, 2011) gives an older age of 18.84 ± 0.02 Ma (McDowell et al. 2014). Lidzbarski reports U-Pb zircon CA-TIMS and CA-SIMS ages that are consistent with these results (Lidzbarski et al. 2012; Lidzbarski 2014).

(3) Post-PST magmatism is represented by epizonal intrusions and small-volume lavas and tuffs. Intrusions include two intra- and pericaldera stocks with a total area of exposure ~30 km², the Moss porphyry (mostly quartz monzodiorite and quartz monzonite) and the Times porphyry (granite), and compositionally diverse porphyry dikes and small plugs that are exposed both within the caldera and within a radius of 10 km (Ransome 1923; Thorson 1971; DeWitt et al. 1986; McDowell et al. 2014). Most dikes and plugs are silicic, but some dikes have intermediate compositions or are composite. The stocks intrude the PST and display clear evidence for magma mingling and likely hybridization, including magmatic enclaves and rounded, rimmed feldspars (McDowell et al. 2014). Magmatic enclaves and rounded phenocrysts of feldspar and quartz are also locally present in the intermediate and silicic dikes (McDowell et al. 2014). U-Pb CA-TIMS zircon ages for the Moss porphyry (18.76 ± 0.11 and 18.84 ± 0.15 Ma) are within error of PST U-Pb zircon and Ar/Ar sanidine ages; Times porphyry and composite dikes that we interpret to be associated with the Moss and Times intrusions range from 18.7 to 18.5 Ma, and a large intracaldera dike is 18.2 Ma (McDowell et al. 2014, zircon CA-TIMS U-Pb).

Post-PST volcanic rocks in the southern Black Mountains consist of ~18.7 to 16.9 Ma intermediate to silicic ignimbrites, block-and-ash flow deposits, lava flows, and volcanogenic sediments (Fig. 1; Faulds et al. 1999; Murphy 2004; Lang et al. 2008; Pearthree et al. 2010; Murphy et al. 2013; McIntosh and

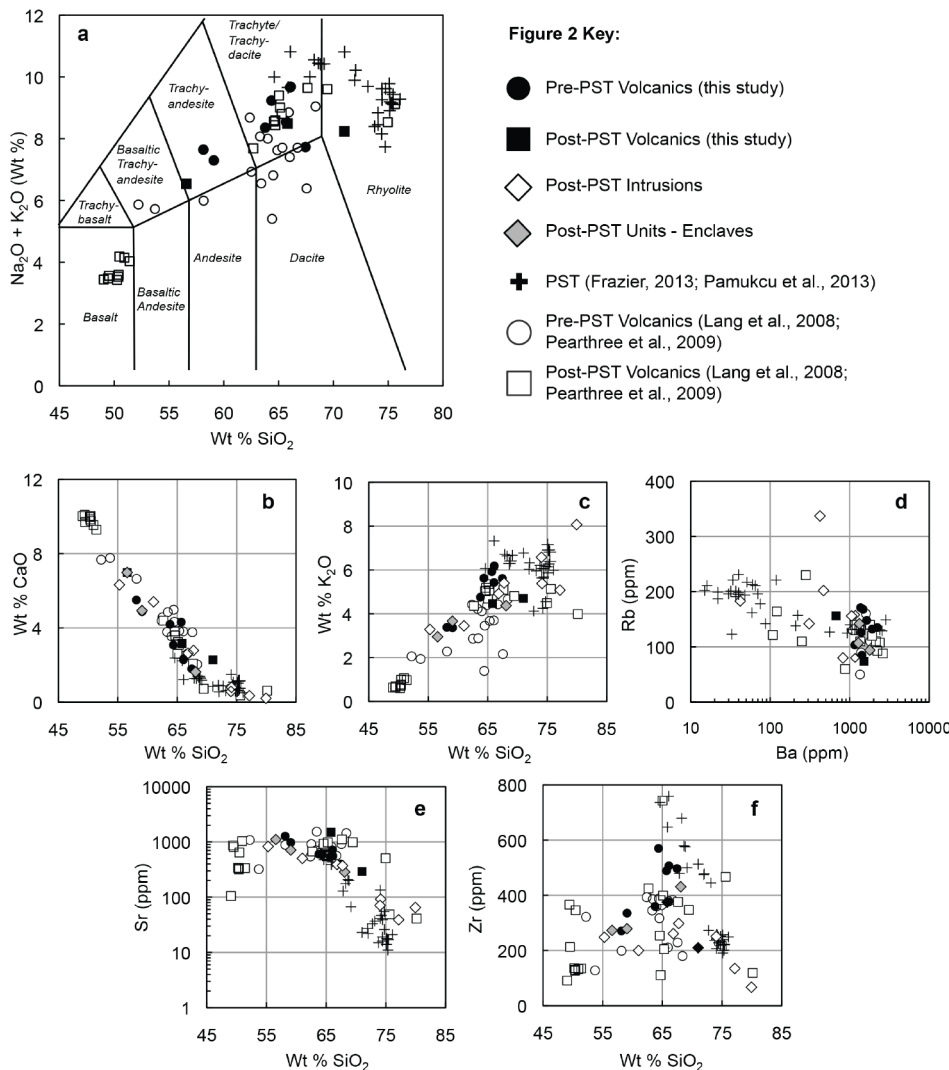


FIGURE 2. Whole-rock compositions of units in the SBMVC (data from this study plus previously published data sets from the SBMVC: [Lang 2001](#); [Lang et al. 2008](#); [Pearthree et al. 2010](#); [Frazier 2013](#); [Pamukcu et al. 2013](#)).

Ferguson, unpublished Ar ages). In this study we investigate two of these units: a prominent, glassy ~18.5 Ma silicic lava (McDowell et al. 2014) and its magmatic enclaves, and a 17.5 Ma intermediate-composition lava containing 2–3 cm euhedral feldspar phenocrysts (McIntosh and Ferguson, unpublished Ar ages).

METHODS

Whole-rock analysis

Elemental compositions. Analyses of 19 representative pre- and post-PST samples from the SBMVC were carried out by Activation Laboratories in Ancaster, Ontario, by INAA, ICP, and ICP-MS (Table 2). Fifteen of these were previously reported in McDowell et al. (2014). For this study, we sent four additional samples to Activation Laboratories and include these in Table 2. We also include analyses of 10 PST samples for which we obtained whole-rock isotopic compositions (eight pumice and fiamme, two enclaves). A total of 33 elemental analyses of PST pumice and fiamme are plotted in Figure 2 (from Pamukcu et al. 2013; Frazier 2013).

Isotopic compositions. We determined whole-rock isotope compositions (Sr, Hf, Nd, and Pb) for the same 19 samples as for elemental analysis, along with 8 PST pumice samples and two enclaves from PST, at the WSU Radiogenic

Isotope and Geochronology Laboratory (RIGL) at Washington State University (Table 3). Approximately 0.25 g of each powdered sample were placed in polytetrafluoroethylene vessels, dissolved in ~7 mL 10:1 HF:HNO₃, and immediately dried at 120 °C to eliminate silica. Samples were then redissolved in ~7 mL 10:1 HF:HNO₃ and placed in steel-jacketed Parr vessels at 150 °C for 5–7 days. The solutions were dried down and redissolved overnight in a mixture of 6 M HCl/H₃BO₃ to convert to chlorides and minimize the production of fluoride species. Samples were dried down again and redissolved in Parr vessels at 150 °C for 24 h in 6 M HCl until sample solutions were clear. These solutions were dried yet again, then redissolved in a mixture of 1 M HCl and 0.1 M HF. High-field-strength elements (including Hf), REE (including Nd), and Sr were initially separated on single cation exchange columns loaded with AG 50W-X12 resin (200–400 mesh). Following the method of Patchett and Tatsumoto (1981), Hf was eluted at the beginning of the procedure in 1 M HCl/0.1 M HF, followed by elution of Sr in 2.5 M HCl and finally bulk REE separation in 6 M HCl. Ti was removed from the Hf fraction, a crucial step, as excess Ti has been shown to alter the measured Hf isotopic composition (Blichert-Toft et al. 1997). Any remaining Yb and Lu in the Hf aliquot were removed in a third stage of column chemistry using 0.18 mL of AG 50W-X12 resin. Sr aliquots were subsequently purified using 0.18 mL Sr-spec resin and HNO₃ (e.g., Gaschnig et al. 2011). Nd was separated from other REEs using LN Spec resin (Gaschnig et al. 2011).

TABLE 2. Whole-rock elemental compositions

Sample Unit Type	SCM-34 1 Pre-PST (Alcyone Trachyte)	SCM-41 2 Pre-PST (Gold Road Trachyte)	WSE-3a 3 Pre-PST (Cook Canyon Tuff)	MLPT-7b 3 Pre-PST (Cook Canyon Tuff)	PSK-6a ^a 4 Pre-PST (Esperanza Trachyte)	PSK-7 4 Pre-PST Lava	PSK-14 4 Pre-PST Lava	PSTG-1C 5 PST Intracaldera Trachyte Fiamma	PST-SWA01A 5 PST Outflow Trachyte Pumice	MLPT-5D 5 PST Outflow Trachyte Pumice
Location ^b	35° 1'52.2"N 114° 27'17.2"W	35° 1'51.3"N 114° 22'30.5"W	34° 54'12.1"N 114° 19'27.4"W	35° 10'35.2"N 114° 4'30.3"W	34° 58'36.3"N 114° 23'1.5"W	34° 59'8.6"N 114° 23'44.2"W	34° 58'28.1"N 114° 23'0.4"W	35° 2'54.9"N 114° 28'31.8"W	34 57'59.5" 114 16'05.7"	34 55'2.0" 114 13'16.7"W
Major oxides, wt%, normalized to 100%										
SiO ₂	64.35	63.77	66.09	67.45	66.05	58.13	59.08	68.82	64.60	67.85
TiO ₂	0.80	0.91	0.76	0.78	0.67	1.03	1.34	0.47	0.59	0.53
Al ₂ O ₃	16.10	16.44	16.04	16.87	17.15	18.29	17.06	16.16	17.28	16.62
Fe ₂ O ₃ (t) ^c	4.53	4.70	3.81	3.74	3.20	5.78	6.84	2.24	4.16	3.04
MnO	0.07	0.09	0.07	0.06	0.05	0.08	0.08	0.07	0.08	0.07
MgO	1.51	1.20	1.00	1.42	0.64	3.03	2.92	0.42	0.78	0.53
CaO	3.08	4.19	2.34	1.80	2.28	5.50	4.87	1.29	2.37	1.28
Na ₂ O	3.61	3.60	3.50	2.12	4.23	4.27	3.93	4.00	3.92	3.29
K ₂ O	5.63	4.76	6.18	5.61	5.43	3.38	3.36	6.41	6.07	6.72
P ₂ O ₅	0.32	0.34	0.20	0.14	0.29	0.50	0.51	0.10	0.14	0.07
(LOI) ^d	1.94	2.62	3.22	6.29	nd ^e	nd6	nd6	0.74	4.20	4.67
(oxide sum) ^e	98.65	97.29	96.86	93.37	97.63	97.20	96.40	96.66	93.52	93.96
Trace elements, ppm										
Sc	8.5	8.4	5.5	6.5	4.4	12.3	15.1	6.1	8.6	8.6
V	60	81	48	44	19	134	123	16	28	20
Ba	2226	1391	1637	1369	1917	1422	1160	1016	2559	560
Rb	135	126	148	171	132	85	104	140	129	127
Sr	590	602	551	398	717	1273	974	199	475	129
Zr	570	360	507	497	376	271	335	576	736	479
Hf	11.1	8.4	12.1	10.5	9.1	6.7	8.3	13.3	13.3	10.2
Y	27	27	24	25	27	23	26	34	26	33
Nb	19.4	22.5	36.4	26.6	27.6	15.6	23.9	21.8	14.3	16.9
Ta	1.1	1.4	1.5	2.0	1.6	0.7	1.4	1.4	1.1	1.3
Ga	21	21	21	21	22	22	22	21	19	20
Cu	12	25	36	8	2	28	20	10	15	10
Zn	91	72	58	69	123	86	82	70	75	65
Pb	29	24	23	22	25	19	21	39	29	31
Th	17.1	19.2	27.5	28.7	12.9	11.8	18.7	19.8	13.3	18.9
U	2.8	3.5	5.0	4.3	2.0	2.7	3.4	4.1	1.9	2.0
La	115	87	103	98	94	91	94	173	133	174
Ce	223	172	198	170	189	179	188	338	236	320
Pr	24.1	18.5	22.0	20.1	20.6	19.9	21.3	35.6	26.9	35.8
Nd	87	66	76	71	74	72	77	106	98	129
Sm	12.7	10.3	11.5	11.0	11.5	11.2	12.4	18.1	13.7	18.8
Eu	2.95	2.14	2.18	1.88	2.75	2.60	2.75	3.14	3.52	2.84
Gd	9.3	7.9	7.6	7.7	7.7	7.3	8.3	10.9	9.0	12.0
Tb	1.10	1.00	0.96	0.93	1.04	0.95	1.09	1.45	1.07	1.39
Dy	5.75	5.36	5.02	4.91	5.49	4.96	5.70	7.60	5.51	7.11
Ho	1.05	1.00	0.94	0.91	1.03	0.92	1.02	1.41	0.98	1.27
Er	2.95	2.84	2.54	2.59	2.66	2.32	2.55	3.93	2.82	3.43
Tm	0.44	0.40	0.37	0.37	0.37	0.32	0.35	0.57	0.40	0.48
Yb	2.81	2.57	2.44	2.39	2.28	1.94	2.08	3.49	2.55	2.98
Lu	0.46	0.41	0.38	0.39	0.35	0.30	0.31	0.50	0.43	0.49

Notes: Samples PSK-6a, PSK-7, and PSK-14 analyzed by WSU lab; all others by XRAL. ^a PSK-6a is from the same lava (Esperanza trachyte) as PSK-11; no elemental analysis available for PSK-11. ^b NAD83. ^c Total Fe as Fe₂O₃. ^d Loss on ignition. ^e Total oxides as analyzed (prior to normalization). ^f nd = LOI not determined.

(Continued on next page)

To minimize Pb blanks, we dissolved additional aliquots of each sample specifically for Pb analysis and, following the approach of [Prytulak et al. \(2006\)](#), separated Pb from solution using Biorad AG1-X8 anion resin. Pb aliquots were then spiked with Tl, to correct for mass fractionation as described by [Gaschnig et al. \(2011\)](#).

Aliquots of each purified species (Sr, Nd, Hf, Pb) were redissolved in 2% HNO₃ for determination of isotopic compositions on the WSU Thermo-Finnigan Neptune MC-ICP-MS. Whole-rock Hf analyses were corrected for mass fractionation using ¹⁷⁹Hf/¹⁷⁷Hf = 0.7325 and normalized using Hf standard JMC475 (¹⁷⁶Hf/¹⁷⁷Hf = 0.282160). Sr analyses were corrected for mass fractionation using ⁸⁶Sr/⁸⁸Sr = 0.1194 and normalized using standard NBS-987 (⁸⁷Sr/⁸⁶Sr = 0.710240). Nd analyses were corrected for mass fractionation using ¹⁴⁶Nd/¹⁴⁴Nd = 0.7219 and normalized using Nd standard Ames (¹⁴³Nd/¹⁴⁴Nd = 0.512138). We corrected for mass bias in the Pb analyses using ²⁰⁵Tl/²⁰³Tl = 2.388 and normalized the mass bias corrected values for standard NBS 981 using ²⁰⁶Pb/²⁰⁴Pb = 16.9405, ²⁰⁷Pb/²⁰⁴Pb = 15.4963, ²⁰⁸Pb/²⁰⁴Pb = 36.7219 ([Galer and Abouchami 1998](#)). ϵ_{Hf} and ϵ_{Nd} were calculated using the CHUR parameters reported by [Bouvier et al. \(2008\)](#).

In situ zircon analyses (oxygen and Lu-Hf)

We performed in situ oxygen isotope and Lu-Hf isotope measurements on zircon from representative pre- to post-PST units: five pre-PST volcanic samples, 13 intrusive post-PST samples, and three volcanic post-PST samples (Supplemental Tables 1 and 2¹). Zircon grains were separated from whole rock using standard methods, including crushing, density separation by water table and heavy liquids, magnetic susceptibility separation by Frantz magnetic separator, and hand-picking. Grains were then mounted in epoxy and polished to their approximate centers and imaged using SEM cathodoluminescence on the JEOL JSM 5600 scanning electron microscope (SEM) at the Microanalysis Center shared by the U.S. Geological Survey and Stanford University.

Oxygen isotopes. Following the methods of Trail et al. (2007), we carried out a total of 467 O isotope analyses (93 pre-PST, 312 post-PST intrusive, 62 post-PST volcanic) at UCLA using the CAMECA IMS 1270 in multi-collection mode (Cs+ primary beam spot size ~20–25 μm). Analyses were calibrated using zircon standard R33, which yielded an in-run reproducibility of 0.48‰. $\delta^{18}\text{O}$ was calculated using VSMOW ([Baertschi 1976](#)). Cited precisions are the geometric

TABLE 2.—CONTINUED

Sample	28556-P1	GJPST-1A	WSWPST-4D	PST01D	WSWPST2A	WSWPST1	PST-NY01A	MP1	MPe1	SCM-38
Unit	5	6	6	6	6	6B	6B	7	8	9
Type	PST	PST	PST	PST	PST	Magnetic Enclave (PST Rhyolite)	Enclave (PST Rhyolite)	Moss Porphyry	Magnetic Enclave (Moss Porphyry)	(Leucogranite) Times Porphyry
Location ^b	34° 54' 14.9"N 114° 19' 41.4"W	35° 14' 14.2"N 114° 22' 13.7"W	34° 53' 30.7"N 114° 22' 18.4"W	35° 11' 19.3"N 114° 21' 12.6"W	34° 53' 24.4"N 114° 22' 19.3"W	34° 53' 43.0"N 114° 22' 21.9"W	35° 17' 18.5"N 115° 13' 38.5"W	35° 6' 36.9"N 114° 27' 6.6"W	35° 6' 35.8"N 114° 27' 3.0"W	35° 2' 8.0"N 114° 27' 23.7"W
Major oxides, wt%, normalized to 100%										
SiO ₂	69.30	72.03	71.94	75.45	75.12	57.61	69.95	66.83	59.07	77.14
TiO ₂	0.46	0.36	0.34	0.20	0.23	1.32	0.48	0.69	1.12	0.17
Al ₂ O ₃	15.39	14.74	14.80	13.14	12.84	16.96	15.53	14.92	16.29	12.21
Fe ₂ O ₃ (t) ^c	2.65	1.83	1.69	1.06	1.40	7.48	2.62	4.27	7.02	1.48
MnO	0.08	0.04	0.05	0.07	0.08	0.07	0.08	0.06	0.08	0.04
MgO	1.11	0.17	0.35	0.20	0.20	2.50	0.32	1.49	3.24	0.14
CaO	1.65	0.55	0.92	0.75	0.61	5.41	0.20	2.64	4.93	0.35
Na ₂ O	2.69	3.89	3.86	2.72	3.63	3.50	4.95	3.97	4.15	3.39
K ₂ O	6.56	6.32	6.03	6.39	5.86	4.59	5.82	4.92	3.67	5.08
P ₂ O ₅	0.13	0.06	0.03	0.03	0.02	0.55	0.05	0.21	0.43	0.00
(LOI) ^d	5.56	0.89	1.46	3.16	0.68	1.82	1.52	2.57	3.26	0.72
(oxide sum) ^e	94.81	99.15	98.34	97.83	96.01	95.98	98.47	95.94	96.58	97.83
Trace elements, ppm										
Sc	6.8	3.2	3.3	3.5	3.6	12.2	7.3	7.6	12.5	8.4
V	18	19	9	< 5	< 5	109	17	62	121	8
Ba	802	87	59	40	40	1943	30	1175	1287	42
Rb	141	142	162	198	195	96	146	158	107	183
Sr	185	22	27	17	18	1514	11	391	712	39
Zr	608	478	475	221	257	400	635	261	279	135
Hf	14.4	11.4	11.8	8.8	8.1	9.0	13.7	6.3	6.4	5.0
Y	34	47	61	33	33	31	52	19	21	21
Nb	31.4	28.3	30.8	39.4	21.5	21.5	35.1	17.2	21.4	31.8
Ta	1.4	2.2	2.3	2.5	2.4	1.3	2.1	1.1	1.3	2.0
Ga	19	20	20	20	18	22	28	20	20	17
Cu	6	3	2	2	10	33	6	14	14	4
Zn	49	46	49	50	46	87	97	57	48	37
Pb	15	25	25	24	24	46	21	19	15	27
Th	22.0	22.2	20.8	32.9	24.5	20.3	19.2	16.7	13.0	33.7
U	2.8	2.8	2.9	6.2	4.1	4.2	3.2	2.6	2.4	4.8
La	147	108	88	70	78	151	159	76	74	48
Ce	298	202	185	124	141	235	236	146	146	88
Pr	32.3	26.7	24.7	13.9	15.6	30.8	37.6	15.6	15.9	7.6
Nd	112	99	96	39	48	104	136	53	57	22
Sm	16.8	20.3	20.8	6.7	8.5	15.8	23.9	8.4	9.3	3.5
Eu	2.66	1.54	1.53	0.567	0.629	3.38	1.41	1.57	2.17	0.22
Gd	11.4	14.1	15.7	5.5	6.5	11.0	14.8	5.8	6.7	3.3
Tb	1.52	2.18	2.50	0.89	1.03	1.20	2.15	0.77	0.94	0.51
Dy	7.58	11.10	13.20	5.20	5.85	5.64	11.50	4.03	4.79	2.97
Ho	1.38	1.96	2.45	1.03	1.19	1.01	2.06	0.78	0.89	0.70
Er	3.81	4.88	6.16	3.17	3.47	2.74	5.78	2.14	2.43	2.27
Tm	0.54	0.73	0.85	0.51	0.55	0.37	0.87	0.31	0.35	0.38
Yb	3.46	3.83	4.79	3.18	3.46	2.35	5.49	2.01	2.20	2.67
Lu	0.54	0.51	0.60	0.47	0.47	0.33	0.86	0.31	0.34	0.44

Notes: Samples PSK-6a, PSK-7, and PSK-14 analyzed by WSU lab; all others by XRAL.^a PSK-6a is from the same lava (Esperanza trachyte) as PSK-11; no elemental analysis available for PSK-11.^b NAD83.^c Total Fe as Fe₂O₃.^d Loss on ignition.^e Total oxides as analyzed (prior to normalization).^f nd = LOI not determined.

(Continued on next page)

mean of the within-spot standard error and the in-run reproducibility on R33. The full data set is reported in Supplemental Appendix 2¹.

Lu-Hf isotopes. Following analyses for O isotopic composition, the mounts were lightly repolished and the age and Lu-Hf isotope composition was determined on a subset of the same grains at RIGL. We conducted a total of 239 analyses of four pre-PST samples (29 analyses), three PST samples (30 analyses), 12 post-PST intrusive samples (139 analyses), and three post-PST volcanic samples (41 analyses).

Analyses were carried out using the laser ablation split-stream method (LASS) whereby U-Pb age and Lu-Hf isotope composition are determined simultaneously (Fisher et al. 2014a). The LASS approach is critical in zircon samples having multiple age components present within single grains, as it allows detection of inadvertent incorporation of ancient zircon domains when targeting younger (i.e., Miocene age) domains (Fisher et al. 2014a, 2014b). Given the young age, and thus low to very low radiogenic Pb concentrations, relatively large analytical uncertainties exist for age determinations, and thus we prefer the higher precision

SIMS age (McDowell et al. 2014).

To constrain the age and Hf isotope composition of the source materials, a small subset of analyses targeted inherited cores (Table 4). When possible, we selected ablation sites that overlapped with previous O isotope analysis locations. Care was taken to avoid placing the laser beam over multiple CL zones. Analyses were calibrated using zircon standards R33 and FC1. The mean ¹⁷⁶Hf/¹⁷⁷Hf for FC1 and R33 [0.282181 ± 36 (2 SD), n = 73; 0.282754 ± 42 (2 SD), n = 112] are in close agreement with the solution MC-ICPMS values of 0.282184 ± 16 (Woodhead and Hergt 2005) and 0.282764 ± 14 (Fisher et al. 2014). Reference zircons 91500 and GJ-1 were analyzed as secondary standards for both U-Pb age and Lu-Hf isotopic composition and are in good agreement with published reference values. Eleven LASS analyses of 91500 yielded a weighted mean ²⁰⁶Pb/²³⁸U age of 1068 ± 12 Ma (2 SE) and a mean ¹⁷⁶Hf/¹⁷⁷Hf of 0.282293 ± 37 (2 SD) (Schoene et al. 2006; Blichert-Toft 2008), while 10 LASS analyses of GJ-1 yielded a weighted mean ²⁰⁶Pb/²³⁸U age of 596 ± 9 Ma (2 SE) and a mean ¹⁷⁶Hf/¹⁷⁷Hf of 0.282015 ± 35 (2 SD) (Morel et al. 2008). Analyses of all reference materials are reported in detail in Supplement Appendix 3¹. ϵ_{Hf} was calculated using CHUR parameters reported by Bouvier et al. (2008). External 2σ precision was $\leq 1.5 \epsilon_{\text{Hf}}$. The full data set is reported in Supplementary Appendix 1¹.

¹ Deposit item AM-16-25127, Supplemental Appendices. Deposit items are free to all readers and found on the MSA web site, via the specific issue's Table of Contents (go to <http://www.minsocam.org/MSA/AmMin/TOC/>).

TABLE 2.—CONTINUED

Sample Unit Type	TIP-1 9 Times Porphyry	SCM-27b 10 Magmatic Enclave (Times Porphyry)	SCM-30 11 Feldspar Dike	SCM-1 11 Porphyry Dike	SIT-1 12 Felsic Lava	SIT-1b 13 Magmatic Enclave (Felsic Lava)	SCM-42 14 Felsic Dike	SCM-5a 14 Felsic Dike	SCM-26 15 Mafic Dike	SIT-2 16 Post-PST (Cottonwood Lava)
Location ^b	35° 4'35.7"N 114° 27'37.5"W	35° 4'7.3"N 114° 26'58.2"W	35° 7'7.8"N 114° 26'2.6"W	35° 4'46.7"N 114° 26'12.1"W	35° 2'34.1"N 114° 20'36.2"W	35° 2'34.3"N 114° 20'36.3"W	35° 1'59.3"N 114° 22'40.3"W	35° 2'55.8"N 114° 26'25.6"W	35° 7'4.5"N 114° 26'18.1"W	35° 2'55.9"N 114° 20'51.9"W
Major oxides, wt%, normalized to 100%										
SiO ₂	74.13	68.08	61.01	67.74	71.00	56.57	74.02	79.93	55.28	65.80
TiO ₂	0.29	0.61	0.85	0.63	0.45	1.14	0.33	0.09	1.13	0.59
Al ₂ O ₃	13.14	15.37	14.85	14.94	14.41	17.14	14.08	10.03	14.97	16.34
Fe ₂ O ₃ (t) ^c	2.13	3.94	5.88	3.87	2.63	7.12	1.66	1.11	8.70	4.56
MnO	0.04	0.07	0.09	0.07	0.05	0.09	0.02	0.02	0.12	0.09
MgO	0.26	1.01	5.18	1.21	0.82	3.91	0.73	0.21	6.11	0.68
CaO	0.80	1.63	5.40	2.78	2.28	6.98	0.58	0.21	6.32	3.16
Na ₂ O	3.80	4.72	3.01	3.16	3.54	3.59	1.95	0.33	3.61	4.03
K ₂ O	5.38	4.37	3.45	5.40	4.70	2.95	6.58	8.07	3.29	4.46
P ₂ O ₅	0.02	0.19	0.28	0.19	0.12	0.49	0.04	0.00	0.47	0.29
(LOI) ^d	0.91	2.00	5.46	3.73	2.89	2.84	2.66	0.83	3.74	0.98
(oxide sum) ^e	98.66	97.65	92.74	95.52	97.23	97.83	98.02	99.90	96.19	97.02
Trace elements, ppm										
Sc	8.5	5.5	15.2	14.0	16.4	17.6	20.0	18.8	8.5	8.4
V	14	35	108	51	36	154	15	8	150	56
Ba	309	1324	823	1059	674	1511	469	423	1167	1789
Rb	142	142	80	156	156	74	202	337	80	94
Sr	92	286	504	372	291	1106	71	65	827	1498
Zr	257	431	200	298	210	273	251	67	248	375
Hf	7.7	9.5	4.7	7.4	5.6	6.2	7.0	3.0	5.9	8.4
Y	29	21	17	26	22	25	25	13	24	18
Nb	27.5	21.1	14.6	23.9	22.1	15.2	28.9	27.7	14.4	15.8
Ta	2.0	1.7	0.8	1.6	1.6	0.8	2.0	2.0	0.8	0.8
Ga	20	20	18	20	18	23	17	10	20	22
Cu	4	4	71	6	6	35	7	6	46	13
Zn	55	71	70	74	40	84	39	11	76	75
Pb	24	28	16	30	25	10	26	13	13	33
Th	26.1	15.2	11.9	19.3	28.5	18.8	29.1	32.7	11.5	25.7
U	3.5	2.2	1.9	3.4	4.6	2.1	4.1	5.7	2.0	3.3
La	85	74	55	79	66	117	74	29	74	128
Ce	157	132	110	153	126	184	144	51	149	247
Pr	15.8	13.2	11.5	16.1	12.5	24.1	14.7	4.2	17.0	25.6
Nd	49	44	42	53	42	87	49	12	63	91
Sm	8.1	6.6	6.9	8.6	6.7	13.5	7.8	1.7	10.6	13.4
Eu	0.89	1.37	1.55	1.45	1.18	2.66	0.97	0.16	2.38	2.99
Gd	5.9	4.8	5.5	6.4	5.5	9.7	5.6	1.6	7.7	9.1
Tb	0.90	0.69	0.68	0.96	0.74	1.17	0.80	0.26	1.04	0.91
Dy	5.10	3.79	3.45	5.18	3.84	5.43	4.68	1.63	5.30	4.03
Ho	1.05	0.75	0.65	1.04	0.78	0.94	0.95	0.38	1.00	0.68
Er	3.07	2.19	1.86	2.89	2.27	2.71	2.78	1.36	2.69	1.93
Tm	0.47	0.33	0.27	0.43	0.35	0.36	0.46	0.27	0.38	0.27
Yb	3.13	2.26	1.70	2.88	2.40	2.18	3.00	2.00	2.32	1.74
Lu	0.50	0.37	0.27	0.45	0.40	0.34	0.50	0.36	0.36	0.27

Notes: Samples PSK-6a, PSK-7, and PSK-14 analyzed by WSU lab; all others by XRAL.^a PSK-6a is from the same lava (Esperanza trachyte) as PSK-11; no elemental analysis available for PSK-11.^b NAD83.^c Total Fe as Fe₂O₃.^d Loss on ignition.^e Total oxides as analyzed (prior to normalization).^f nd = LOI not determined.

RESULTS

Whole-rock geochemistry documents SBMVC magmatic evolution from predominantly intermediate-composition effusive volcanism (pre-PST), to a high-volume high-silica explosive event (PST), and finally to compositionally diverse volcanic and intrusive magmatism (post-PST). Pre-PST volcanic rocks have 48 to 70 wt% SiO₂; post-PST intrusions, 55 to 80 wt%; and post-PST volcanic rocks, 48 to 75 wt% (Lang et al. 2008; Pearthree et al. 2010; Frazier 2013; McDowell et al. 2014; Fig. 2; Tables 1 and 2). True mafic rocks (basalts and gabbros) are relatively rare, and, except for PST, Times porphyry, and minor dikes and stocks, rhyolites, and granites are also uncommon. The dominant SBMVC intermediate rocks are rich in total alkalis and especially in K₂O and almost all are basaltic trachyandesite, trachyandesite, and trachydacite or

trachyte in the classification scheme of Le Bas et al. (1986). Most samples fall in the trachyte plus trachydacite field and are trachytes according to the criterion normative Qz/(Qz+Pl+Or) < 0.2, and therefore for simplicity we use the term “trachyte” as a general descriptor. Pre- and post-PST units are elementally distinct from the PST, which has lower Sr and Ba and higher Zr and Rb at a given SiO₂ than its magmatic predecessors and successors (Fig. 2).

Sr, Nd, and Hf isotopic ranges for pre-PST units (⁸⁷Sr/⁸⁶Sr = 0.7093 to 0.7110, ε_{Nd} = -8.3 to -11.6, and ε_{Hf} = -8.2 to -14.0) are similar to those of post-PST volcanics and intrusions (⁸⁷Sr/⁸⁶Sr = 0.7091 to 0.7124, ε_{Nd} = -8.4 to -10.4, and ε_{Hf} = -8.8 to -13.1) (Table 3, Fig. 3). Times and Moss magmatic enclaves (SCM-27b and MPe1, respectively) have the most primitive isotopic ratios (e.g., highest ε_{Hf} and ε_{Nd}). Throughout

TABLE 3. Whole-rock isotopic compositions (Pb, Nd, Hf, Sr)

Sample Unit name no.	Unit	Pb				Nd				Hf				Sr							
		$^{206}\text{Pb}/^{204}\text{Pb}$	\pm	$^{207}\text{Pb}/^{204}\text{Pb}$	\pm	$^{208}\text{Pb}/^{204}\text{Pb}$	\pm	$^{143}\text{Nd}/^{144}\text{Nd}$	\pm	εNd^a	2SE	$^{176}\text{Hf}/^{177}\text{Hf}$	\pm	εHf^b	2SE	$^{87}\text{Sr}/^{86}\text{Sr}_{\text{src}}$	\pm	$^{87}\text{Rb}/^{86}\text{Sr}$	$^{87}\text{Sr}/^{86}\text{Sr}_{\text{init}}$		
SIT-2	16	Post-PST (Cottonwood Lava)	18.4259	0.0038	15.6134	0.0032	39.1487	0.0075	0.512104	14	-10.3	0.3	0.282414	6	-13.1	0.2	0.709818	8	0.177	0.709771	
SCM-26	15	Mafic Dike	18.4916	0.0023	15.6248	0.0022	39.2864	0.0053	0.512104	13	-10.3	0.3	0.282450	6	-11.8	0.2	0.710188	10	0.273	0.710115	
SCM-5a	14	Felsic Dike	18.3573	0.0039	15.6065	0.0033	39.2777	0.0077	0.512171	14	-9.0	0.3	0.282510	6	-9.7	0.2	0.715932	8	14.636	0.712024	
SCM-42	14	Felsic Dike	18.3134	0.0023	15.6104	0.0022	39.1214	0.0054	0.512155	13	-9.3	0.3	0.282479	6	-10.8	0.2	0.713239	8	8.032	0.711095	
SIT-1b	13	Magmatic Enclave (Felsic Lava)	18.3176	0.0023	15.6029	0.0022	38.9525	0.0054	0.512157	13	-9.2	0.3	0.282501	6	-10.0	0.2	0.709176	8	0.189	0.709126	
SIT-1	12	Felsic Lava	18.2477	0.0027	15.6033	0.0026	39.1237	0.0061	0.512155	14	-9.3	0.3	0.282498	6	-10.2	0.2	0.710537	16	1.513	0.710133	
SCM-1	11	Feldspar Porphyry Dike	18.2755	0.0027	15.6019	0.0026	39.0810	0.0061	0.512143	14	-9.5	0.3	0.282487	6	-10.5	0.2	0.710462	8	1.184	0.710146	
SCM-30	11	Feldspar Porphyry Dike	18.2449	0.0023	15.5986	0.0022	39.0085	0.0054	0.512194	12	-8.5	0.2	0.282536	6	-8.8	0.2	0.709579	10	0.448	0.709460	
SCM-27b	10	Magmatic Enclave (Times Porphyry)	18.3021	0.0038	15.6048	0.0032	39.0608	0.0077	0.512208	14	-8.2	0.3	0.282535	6	-8.8	0.2	0.710034	8	1.402	0.709660	
TIP-1	9	Times Porphyry	18.2894	0.0038	15.6087	0.0032	39.1201	0.0075	0.512134	14	-9.7	0.3	0.282456	6	-11.6	0.2	0.711322	8	4.357	0.710158	
SCM-38	9	(Leuocanrite) Times Porphyry	18.2842	0.0039	15.6049	0.0032	39.0954	0.0077	0.512126	14	-9.8	0.3	0.282450	6	-11.8	0.2	0.715925	8	13.246	0.712388	
MPe1	8	Magmatic Enclave (Moss Porphyry)	18.2864	0.0039	15.6064	0.0033	39.1196	0.0078	0.512197	14	-8.4	0.3	0.282511	6	-9.7	0.2	0.710422	6	0.424	0.710309	
MP1	7	Moss Porphyry	18.2692	0.0038	15.6062	0.0032	39.1173	0.0076	0.512104	15	-10.3	0.3	0.282446	6	-12.0	0.2	0.711181	6	1.141	0.710876	
PST-NY01A	6B	Enclave (PST Rhyolite)	18.3723	0.0038	15.6035	0.0032	39.2262	0.0076	0.512256	14	-7.3	0.3	0.282576	6	-7.4	0.2	0.726228	18	37.469	0.716224	
WS	WPST1	6B	Magmatic Enclave (PST Rhyolite)	18.2610	0.0027	15.5886	0.0026	39.0224	0.0062	0.512215	15	-8.1	0.3	0.282539	6	-8.7	0.2	0.709107	8	0.179	0.709059
WS	WPST2a	6	PST Outflow Rhyolite Pumice	18.2859	0.0038	15.6150	0.0031	39.2030	0.0074	0.512045	14	-11.4	0.3	0.282392	6	-13.9	0.2	0.720019	6	30.583	0.711854
PST01D	6	PST Outflow Rhyolite Pumice	18.2600	0.0039	15.6092	0.0033	39.2053	0.0077	0.512039	13	-11.5	0.3	0.282396	6	-13.8	0.2	0.731594	6	32.880	0.722815	
WS	WPST-4D	6	PST Outflow Rhyolite Pumice	18.2590	0.0022	15.6725	0.0021	39.3266	0.0051	0.512042	13	-11.5	0.3	0.282390	6	-14.0	0.2	0.715762	22	16.938	0.711240
GJPST-1A	6	PST Outflow Rhyolite Pumice	18.2181	0.0022	15.6013	0.0021	39.0842	0.0051	0.512050	13	-11.3	0.3	0.282388	6	-14.0	0.2	0.715661	12	18.221	0.710796	
28556-P1	5	PST Outflow Trachyte Pumice	18.2181	0.0022	15.6038	0.0021	39.1400	0.0052	0.512050	12	-11.3	0.2	0.282388	6	-14.0	0.2	0.711795	10	2.152	0.711221	
MLPT-5D	5	PST Outflow Trachyte Pumice	18.2317	0.0023	15.6040	0.0021	39.1165	0.0053	0.512047	12	-11.4	0.2	0.282395	6	-13.8	0.2	0.712358	10	2.779	0.711616	
PST-SWA-01A	5	PST Outflow Trachyte Pumice	18.2044	0.0038	15.6022	0.0032	39.0985	0.0076	0.512037	15	-11.6	0.3	0.282380	6	-14.3	0.2	0.711454	6	0.767	0.711249	
PSTG-1C	5	PST Intracaldera Trachyte Fiamma	18.2584	0.0038	15.6083	0.0032	39.1031	0.0076	0.512047	15	-11.4	0.3	0.282385	6	-14.2	0.2	0.712586	6	1.986	0.712056	
PSK-14	4	Pre-PST Lava	18.4513	0.0028	15.6173	0.0026	39.1675	0.0062	0.512212	14	-8.2	0.3	0.282552	6	-8.2	0.2	0.709334	10	0.300	0.709254	
PSK-7	4	Pre-PST Lava	18.4072	0.0028	15.6157	0.0026	39.1719	0.0062	0.512083	14	-10.7	0.3	0.282415	6	-13.1	0.2	0.710075	10	0.188	0.710025	
PST-11d	4	Pre-PST (Esperanza Trachyte)	18.3476	0.0022	15.6089	0.0022	39.0053	0.0051	0.512193	14	-8.5	0.3	0.282502	6	-10.0	0.2	0.709442	14	0.521	0.709303	
WSE3a	3	Pre-PST (Cook Canyon Tuff)	18.2833	0.0038	15.6050	0.0033	39.0605	0.0081	0.512122	12	-9.9	0.2	0.282465	6	-11.3	0.2	0.710378	10	0.758	0.710175	
SCM-41	2	Pre-PST (Gold Road Trachyte)	18.3754	0.0038	15.6149	0.0032	39.1828	0.0075	0.512127	14	-9.8	0.3	0.282461	6	-11.5	0.2	0.710524	8	0.591	0.710367	
SCM-34	1	Pre-PST (Alcyone Trachyte)	18.1867	0.0028	15.5984	0.0027	39.0465	0.0066	0.512041	14	-11.5	0.3	0.282390	6	-14.0	0.2	0.711154	8	0.646	0.710982	

^a ε_{Nd} calculated using present day CHUR: $^{143}\text{Nd}/^{144}\text{Nd} = 0.512638$ (Bouvier et al. 2008).^b ε_{Hf} calculated using present day CHUR: $^{176}\text{Hf}/^{177}\text{Hf} = 0.282785$ (Bouvier et al. 2008).^c Ratios calculated from ICP-MS trace element data.^d Sample from same unit as PSK-6a in Table 2 (no elemental analysis available for PST-11); location: 34° 58' 50.0"N, 114° 23' 23.0"W.

Analysts: S.M. McDowell, W.O. Frazier, and C.M. Fisher.

TABLE 4. Proterozoic zircon (U-Pb ages, Hf, and O isotopic compositions)

Rock unit and analysis number	$^{207}\text{Pb}/^{235}\text{U}$ age (Ma)	1σ	$^{206}\text{Pb}/^{238}\text{U}$ age (Ma)	1σ	$^{207}\text{Pb}/^{206}\text{Pb}$ age (Ma)	1σ	Present day ϵ_{Hf}	$\delta^{18}\text{O}$
Gold Road Trachyte								
SCM41_4	1636	18	1618	28	1676	16	-30	7.9
SCM41_5	1607	18	1509	26	1752	15	-30	5.7
Peach Spring Tuff								
MLPT5D_11	1569	15	1520	22	1664	12	-33	nd
Moss Porphyry								
SCM6_7	1638	19	1611	30	1687	15	-33	nd
MPe1Ne_9	1689	20	1714	31	1673	22	nd	nd
Feldspar Porphyry Dike								
SCM30_22	1636	17	1593	26	1699	14	-33	nd

Notes: nd = not determined; 16 additional analyses revealed evidence for Proterozoic zircon during the ablation but are not reported owing to too few ratios to reliably determine either age or Hf isotopic composition.

the sample suite, ϵ_{Nd} shows a strong positive correlation with ϵ_{Hf} . All pre- and post-PST units have Pb isotopic ratios within the ranges $^{206}\text{Pb}/^{204}\text{Pb} = 18.19\text{--}18.49$, $^{207}\text{Pb}/^{204}\text{Pb} = 15.60\text{--}15.62$, and $^{208}\text{Pb}/^{204}\text{Pb} = 38.95\text{--}39.29$. PST samples are more uniform isotopically and generally have lower ϵ_{Nd} and ϵ_{Hf} and higher $^{87}\text{Sr}/^{86}\text{Sr}_i$ than the other SBMVC rocks [$^{87}\text{Sr}/^{86}\text{Sr}_i = 0.7108$ to 0.7121 (with one higher outlier, see discussion)], $\epsilon_{\text{Nd}} = -11.4$ to -11.6 , and $\epsilon_{\text{Hf}} = -13.8$ to -14.2 ; Pb isotope ratios are similar to those of the rest of the SBMVC ($^{206}\text{Pb}/^{204}\text{Pb} = 18.20\text{--}18.29$, $^{207}\text{Pb}/^{204}\text{Pb} = 15.60\text{--}15.62$, and $^{208}\text{Pb}/^{204}\text{Pb} = 39.09\text{--}39.32$). Collectively, SBMVC units have isotopic signatures consistent with those determined for other Miocene intrusive and volcanic units within the northern CREC (e.g., Miller and Wooden 1994; Metcalf et al. 1995; Falkner et al. 1995; Miller et al. 2000; Bachl et al. 2001; Erickson et al. 2004) (Fig. 3).

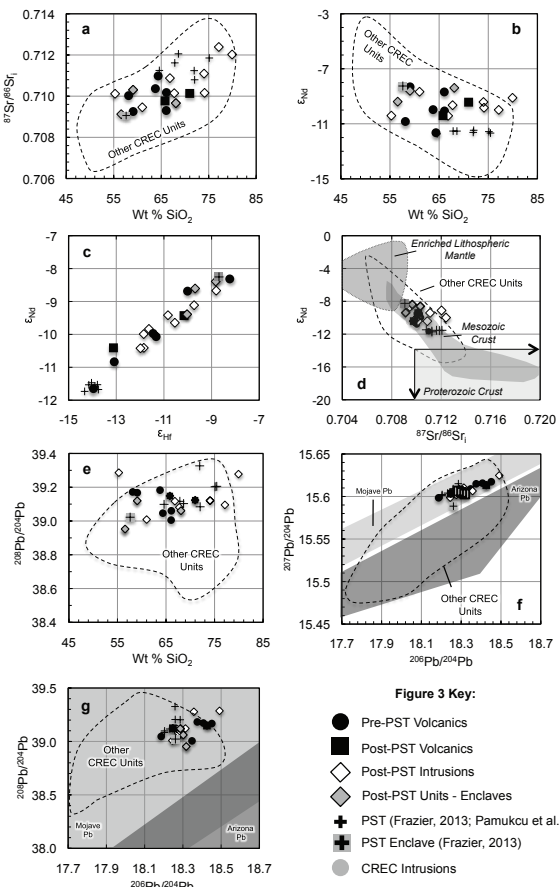
Zircon $\delta^{18}\text{O}$ in the majority of pre-PST, PST, and post-PST units falls within the range +5 to +7.3‰, with several higher outliers between $\delta^{18}\text{O} = +7.8$ to +8.8 (one extreme outlier has $\delta^{18}\text{O} = +12.2$) and lower outliers between +4.2 to +5.0 (Fig. 4). Broadly, zircon $\delta^{18}\text{O}$ decreases from older to younger units: average $\delta^{18}\text{O} = +6.8$ in the oldest sample, ~19 Ma Alcyone trachyte, whereas average $\delta^{18}\text{O} = +5.6$ in the youngest samples, ~18.2 Ma silicic porphyry dikes (Fig. 4). PST values, excluding one lower outlier at 4.5‰, range from 5.6 and 7.2‰ and average 6.4‰.

The 239 LASS zircon spots interpreted to be of Miocene age yielded ϵ_{Hf} values that range from -6 to -16 (Fig. 4). Overall, ϵ_{Hf} is higher in post-PST units than in pre-PST units. The oldest sample, Alcyone trachyte, and the PST have the lowest values (near -14). All samples younger than PST have some zircons with $\epsilon_{\text{Hf}} > -10$, whereas all analyzed zircons from PST or pre-PST units have $\epsilon_{\text{Hf}} < -10$.

Six LASS analyses of zircons from five samples clearly reveal inheritance: their $^{206}\text{Pb}/^{238}\text{U}$ and $^{207}\text{Pb}/^{206}\text{Pb}$ ages are 1.51–1.62 and 1.66–1.75 Ga, respectively, and ϵ_{Hf} values are -30 to -34 (Table 4).

For most paired O and Hf analyses, obtained from the same areas of single zircon grains, ϵ_{Hf} correlates negatively with $\delta^{18}\text{O}$ (Table 5; Fig. 5a). This correlation breaks down for zircons with the lowest, near- and sub-mantle, $\delta^{18}\text{O} (< 5.5\text{\textperthousand})$. All of the low- $\delta^{18}\text{O}$ zircon analyses are from post-PST intrusive units, with exception of the single outlier PST grain.

Ranges of measured ϵ_{Hf} values in individual samples (excluding analyses that we interpret to have partly or entirely

**Figure 3 Key:**

- Pre-PST Volcanics
- Post-PST Volcanics
- ◇ Post-PST Intrusions
- ◆ Post-PST Units - Enclaves
- ✚ PST (Frazier, 2013; Pamukcu et al., 2013)
- ✚ PST Enclave (Frazier, 2013)
- CREC Intrusions

FIGURE 3. Whole-rock isotopic compositions of pre- to post-PST SBMVC units (this study); CREC intrusions (Falkner et al. 1995, Bachl et al. 2001, and unpublished Vanderbilt and San Jose State University data). Strontium-neodymium isotopic fields: inferred enriched mantle composition (Feuerbach et al. 1993); Proterozoic and Mesozoic rocks of the region (Bennett and DePaolo 1987; Miller and Wooden 1994; Allen et al. 1995; Kapp et al. 2002). Lead isotopic fields for Mojave and Arizona terranes are from Wooden et al. (1988), Wooden and Miller (1990), and Feuerbach et al. (1998).

encountered inherited cores) are 3 to 7 units, in many cases exceeding $\pm 2\sigma$ analytical uncertainty. Similarly, $\delta^{18}\text{O}$ displays one- to four-unit intrasample variation, also commonly exceeding analytical uncertainty (see Fig. 5b).

DISCUSSION

Whole-rock Sr-Nd-Hf-Pb isotopes

Whole-rock isotopic ratios serve to constrain contributions from potential sources for Miocene magmas in the CREC (Fig. 3). The Proterozoic crust of this region is characterized by high to very high $^{87}\text{Sr}/^{86}\text{Sr}$ (>0.710 , up to 0.80 and higher) and low to very low ϵ_{Nd} (~ -15 to -22); Paleoproterozoic rocks in general, especially the more silicic rocks, are concentrated in the upper and lower portions of these ranges of values, respectively, whereas Mesoproterozoic rocks fall in the lower and upper portions (Bennett and DePaolo 1987; Miller and Wooden 1994). We are unaware of published whole-rock Hf isotope data for Proterozoic rocks in this area, but, based on the $\epsilon_{\text{Nd}}-\epsilon_{\text{Hf}}$ correlations of the Crustal and Terrestrial Arrays (Vervoort et al. 1999, 2011) and present day ϵ_{Nd} of Proterozoic rocks in and near the CREC, we estimate that their ϵ_{Hf} values range from ~ -17 to -33 . Numerous studies have concluded that juvenile, mantle-derived magmas in the CREC and environs older than ~ 12 Ma, were derived from ancient enriched lithospheric mantle [$\epsilon_{\text{Nd}} < \sim 4$, $^{87}\text{Sr}/^{86}\text{Sr} > \sim 0.705$; e.g., Daley and DePaolo 1992; DePaolo and Daley 2000; Feuerbach et al. 1993; Metcalf et al. 1995 (also see Metcalf et al. op. cit. for a rare exception)]. More silicic igneous rocks of Mesozoic and Cenozoic age span the Nd-Sr, and presumably Hf, isotopic range between what is thought to be the enriched regional lithospheric mantle and Proterozoic crust (Fig. 3) and are generally interpreted to reflect hybridization processes involving these two sources (e.g., Miller and Wooden 1994; Allen et al. 1995; Bachl et al. 2001).

Lead isotope ratios for almost all mid-Miocene and older rocks in this region fall above the Northern Hemisphere Regression Line (elevated $^{207}\text{Pb}/^{204}\text{Pb}$ and $^{208}\text{Pb}/^{204}\text{Pb}$ relative to $^{206}\text{Pb}/^{204}\text{Pb}$). Wooden and coworkers (Wooden et al. 1988; Wooden and Miller 1990; see also Feuerbach et al. 1998) have identified two Pb isotopic provinces: the Mojave province to the west is characterized by higher $^{207}\text{Pb}/^{204}\text{Pb}$ and $^{208}\text{Pb}/^{204}\text{Pb}$ than the Arizona province (Fig. 3). The boundary between the two provinces is thought to lie within the CREC, very near the SBMVC.

Sr_i and Nd isotope ratios for SBMVC samples overlap with those of other Miocene units within the CREC (Sr_i ≈ 0.709 to 0.714, $\epsilon_{\text{Nd}} \approx -8$ to -15) (Fig. 3d). Like other CREC igneous units, isotopic signatures of SBMVC volcanics and intrusions suggest that they are mixtures of juvenile and crustal components, derived, respectively, from the regional enriched lithospheric mantle and the Proterozoic crust. The wide range of isotopic compositions implies a wide range of proportions of the two types of contributing materials. The less evolved compositions (lower Sr_i, higher ϵ_{Nd}) permit a very high proportion of juvenile material, but the range of suggested compositions of purely juvenile magmas leaves unclear whether the less isotopically evolved SBMVC rocks could be derived entirely from the mantle or have a substantial crustal component. A great majority of analyzed samples lie in a swath between plausible mantle and crustal sources, which we interpret to indicate hybridization involving large, varying crustal and mantle fractions. Isotopic data for Mesozoic igneous units in and near the CREC overlap with those of the SBMVC (e.g., Miller and Wooden 1994; Gerber et al. 1995) and could therefore represent plausible crustal

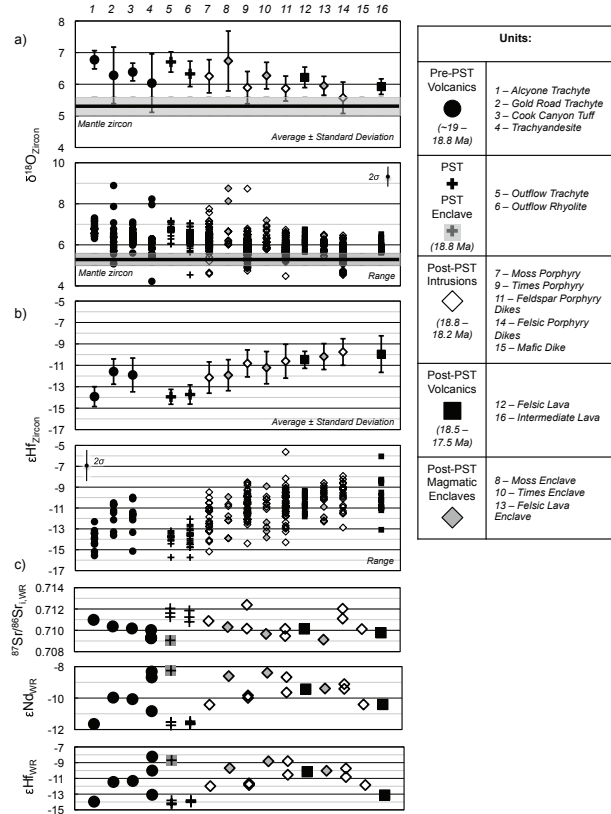


FIGURE 4. Plots of zircon and whole rock isotopic data for pre-PST units (left-hand side of graphs) to post-PST units (right-hand side of graphs). Numbers along the top of the graphs correlate with unit numbers in Table 1, which represent a general time sequence from pre- to post-PST. (a) Oxygen isotopes in zircon. Top graph shows average values and standard deviations; bottom graph shows full range of zircon $\delta^{18}\text{O}$ for each sample. Range of mantle zircon ($\delta^{18}\text{O} = +5.5 \pm 0.3\text{\textperthousand}$) shown for comparison. (b) Hafnium isotopes in zircon. Top graph shows average values and standard deviations; bottom graph shows full range of zircon ϵ_{Hf} for each sample. (c) Whole-rock ϵ_{Nd} , ϵ_{Hf} , and $^{87}\text{Sr}/^{86}\text{Sr}_i$ for all SBMVC units. Hf isotope measurements that yielded concurrently measured mixed U-Pb ages (i.e., discordant) are excluded from Figures 4 and 5.

sources that do not require hybridization with juvenile material. However, because the southern Black Mountains lack exposures of Mesozoic rocks, and extensive zircon dating has found no evidence of Mesozoic inheritance (McDowell et al. 2014; Lidzbarski et al. 2012; Lidzbarski 2014; this study), we infer that Mesozoic-age crust did not serve as a significant contributor to SBMVC magmas.

Lead isotope ratios strongly suggest that SBMVC magmas were derived from the regional lithosphere (crust and mantle). More specifically, uniformly high $^{207}\text{Pb}/^{204}\text{Pb}$ and $^{208}\text{Pb}/^{204}\text{Pb}$ indicate origin within Mojave, not Arizona, province lithosphere (Fig. 3).

The PST, including both trachyte and rhyolite, and Alcyone trachyte have isotopic compositions that suggest the largest Paleoproterozoic crustal components among all sampled units. One outflow PST rhyolite pumice has much higher Sr_i of

TABLE 5. Paired O and Hf isotopic analyses of zircon

Sample number	ϵ_{Hf}	$\delta^{18}\text{O}$	Sample number	ϵ_{Hf}	$\delta^{18}\text{O}$			
Pre-PST Trachyte: Alcyone								
SCM34_1_20	-12.3	6.6	MLPT5D_9_11	-14.1	6.9			
SCM34_2_19	-13.9	6.8	MLPT5D_10_10	-13.8	6.7			
SCM34_4_18	-14.4	6.3	MLPT5D_14_9	-13.8	6.1			
SCM34_5_11	-14.5	7.2	MLPT5D_15_8	-13.5	6.7			
SCM34_11_7	-13.2	6.8	Moss Porphyry					
SCM34_10_4	-14.0	6.6	SCM6_1_1	-13.3	6.2			
SCM34_1_8	-12.3	6.6	SCM6_7_12	-33.4	6.9			
Pre-PST Trachyte: Gold Road								
SCM41_1_1	-10.6	5.9	MP1_1-1	-15.2	7.1			
SCM41_4_3	-29.7	7.9	MP1_9_13	-10.5	6.1			
SCM41_5_2	-29.7	5.7	MPe1Ne_1_2	-10.0	6.6			
SCM41_8_7	-13.3	6.4	MPe1Ne_18_12	-11.0	6.5			
SCM41_9_6	-10.5	5.7	MPe1ne_17_16	-12.8	6.2			
SCM41_12_12	-12.1	6.6	MPe1Ne_5_17	-13.2	6.4			
SCM41_13_11	-11.2	6.4	MPe1Ne_7_21	-12.5	6.1			
SCM41_10_10	-13.6	5.7	MPene1_1_2	-10.0	6.6			
Cook Canyon Tuff								
MLPT7A_1_10	-11.6	6.5	Moss Porphyry enclave					
MLPT7A_2_7	-11.6	6.2	MPe1_10_12	-13.9	6.2			
MLPT7B_9_1	-10.0	6.4	MPe1_14_16	-33.3	6.6			
MLPT7B_7_9	-11.8	6.4	Times Granite					
MLPT7B_4_15	-12.1	6.1	SCM20_1_1	-10.4	6.3			
MLPT7B_1_10	-11.4	6.3	SCM20_2_3	-9.8	6.0			
MLPT7B_2_18	-13.3	6.5	SCM20_4_7	-8.5	6.4			
Peach Spring Tuff Rhyolite								
MLPT2H_11_3	-13.2	6.4	SCM20_6_14	-11.7	6.0			
MLPT2H_9_11	-13.4	6.1	SCM20_8_16	-10.2	6.0			
MLPT2H_7_15	-15.7	6.5	SCM20_9_19	-9.9	6.5			
MLPT2H_8_10	-13.4	6.2	SCM20_10_20	-11.4	6.5			
MLPT2H_6_19	-14.5	6.3	SCM20_12_28	-10.5	6.1			
MLPT3B_12_2	-12.1	6.5	TIP1_3_1	-10.0	5.8			
MLPT3B_10_5	-14.5	6.3	TIP1_5_3	-12.3	5.5			
MLPT3B_8_6	-14.8	6.6	TIP1_6_5	-14.4	6.2			
MLPT3B_5_14	-13.9	6.3	TIP1_8_13	-12.1	6.1			
MLPT3B_3_16	-14.3	6.1	TIP1_10_27	-12.1	6.2			
MLPT3B_4_15	-14.1	6.3	TIP1_12_28	-10.6	5.9			
MLPT3B_1_18	-13.6	6.3	SCM37_3_19	-11.2	4.9			
MLPT3B_7_13	-13.1	4.5	SCM37_4_20	-12.6	5.2			
Peach Spring Tuff Trachyte								
MLPT5D_3_19	-15.7	6.8	SCM37_5_18	-8.8	4.7			
MLPT5D_5_16	-14.0	6.8	SCM37_8_14	-8.6	4.9			
Times Granite enclave								
SCM27B_2_2	-10.6	6.0	SCM37_15_11	-9.9	5.6			
SCM27B_5_12	-11.1	6.7	SCM37_13_1	-11.6	5.8			
SCM27B_6_11	-13.8	6.3	SCM37_4_20	-12.6	5.2			
SCM27B_9_17	-10.2	6.1	Felsic Porphyry Dike					
SCM27B_10_18	-8.9	6.3	SCM30_9_10	-11.2	6.0			
SCM27B_1_1	-10.9	5.8	SCM30_16_6	-10.0	5.8			
SCM27B_4_6	-10.6	5.8	SCM30_11_1	-10.5	5.9			
Feldspar Porphyry Dike								
SCM5A_4_9	-9.1	5.9	SCM30_12_2	-10.8	5.6			
SCM5A_5_11	-12.9	6.1	SCM30_10_7	-11.0	5.8			
SCM5A_6_12	-8.2	5.7	SCM30_20_20	-9.9	5.6			
SCM5A_7_14	-9.1	5.2	Post-PST Felsic Lava					
SCM5A_8_17	-9.9	5.9	SIT1_2_1	-11.8	6.1			
SCM5A_1_1	-11.5	6.0	SIT1_3_2	-10.8	6.2			
BCD_1_20	-9.2	5.2	SIT1_4_8	-10.6	5.7			
BCD_3_14	-9.1	5.0	SIT1_6_9	-9.9	6.1			
BCD_4_13	-10.1	4.6	SIT1_8_10	-10.8	6.1			
BCD_5_11	-11.3	5.4	SIT1_11_12	-9.9	6.4			
BCD_7_9	-9.2	5.6	Post-PST Felsic Lava enclave					
BCD_12_1	-9.0	6.1	SIT1B_1_2	-12.2	5.7			
BCD_10_4	-7.9	5.4	SIT1B_3_3	-9.5	6.2			
BCD_3_14	-9.1	5.0	SIT1B_4_5	-9.1	6.1			
Felsic Porphyry Dike								
SCM1B_1_1	-8.8	5.8	SIT1B_16_10	-9.9	6.3			
SCM1B_3_2	-11.7	6.3	SIT1B_17_12	-10.2	5.9			
SCM1B_4_3	-10.9	5.8	SIT1B_9_14	-10.9	6.5			
SCM1B_8_18	-14.3	6.5	SIT1B_12_18	-11.9	6.1			
SCM1B_10_21	-9.8	6.1	SIT1B_11_17	-12.3	6.4			
SCM13_2_18	-10.0	5.6	SIT1B_14_20	-10.2	6.0			
SCM13_6_14	-10.6	5.4	SIT1B_8_13	-9.7	5.8			
SCM13_7_13	-9.4	5.8	Post-PST Intermediate Lava					
SCM13_8_12	-11.5	5.6	SIT2_14_16	-10.9	6.0			
			SIT2_13_15	-10.3	5.7			
			SIT2_11_13	-8.6	6.1			
			SIT2_12_14	-10.3	5.8			
			SIT2_10_12	-11.2	6.3			
			SIT2_8_10	-8.4	6.4			
			SIT2_6_8	-8.3	6.5			

(Continued on next page)

TABLE 5.—*CONTINUED*

Sample number	ϵ_{Hf}	$\delta^{18}\text{O}$	Sample number	ϵ_{Hf}	$\delta^{18}\text{O}$
Felsic Porphyry Dike					
SCM13_11_9	-9.5	5.9	SIT2_5_7B	-9.5	6.1
SCM13_13_8	-8.2	5.7	SIT2_4_5	-13.1	5.8
SCM13_12_7	-5.6	5.7	SIT2_3_2	-10.9	5.9
SCM13_14_5	-9.1	6.0	SIT2_2_3	-10.9	5.6
SCM13_15_4	-12.7	5.9	SIT2_1_4	-9.9	5.7
SCM13_16_1	-9.2	5.2			
SCM13_4_17	-10.8	5.5			
SCM30_21_18	-11.8	5.9			
SCM30_19_16	-9.8	5.8			

Notes: Sample designations follow this protocol: SCM34_“X”_“Y”; where “X” = Hf spot number and “Y” = O spot number in Supplementary data files¹. External precision on ϵ_{Hf} is 1.5 ϵ_{Hf} units (2 SD) based on repeated analyses of well-characterized standard, R33 and FC1 (Fisher et al. 2014). External precision for O varied over the course of the analytical sessions from 0.1 to 0.38 (1 SD) based on repeated analyses of standard R33. Complete results including all errors are presented in the Supplementary data files¹.

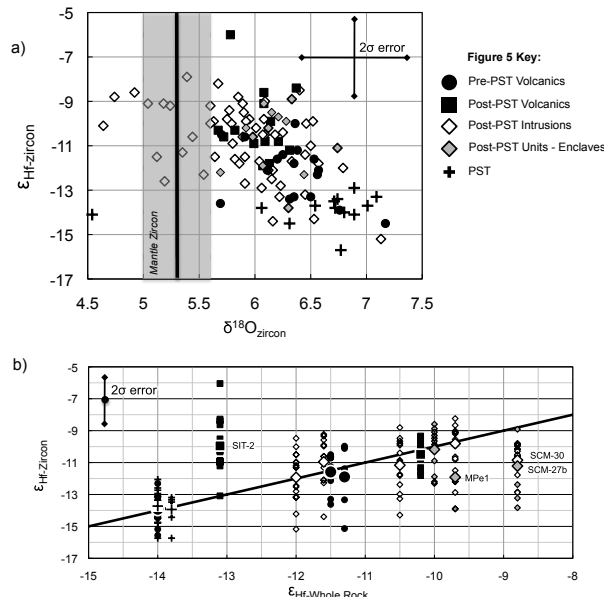


FIGURE 5. Zircon oxygen and hafnium isotope data from SBMVC units. (a) Subset of analyses representing paired O and Hf analyses obtained from the same areas in single grains. (b) Whole-rock ϵ_{Hf} vs. zircon ϵ_{Hf} for pre- to post-PST units. Line shows trend of equal whole rock and zircon ϵ_{Hf} .

0.723; this sample, like other PST rhyolites, has very low Sr concentration (17 ppm), and we attribute the high Sr_i to slight contamination through incorporation of a few percent of Proterozoic crust with much higher ⁸⁷Sr/⁸⁶Sr and Sr concentration (Miller and Wooden 1994), perhaps as a lithic fragment. Other pre- and post-PST extrusive and intrusive units display a wider range of whole-rock isotopic values and have more primitive isotopic compositions on average (Fig. 3). Lower-SiO₂ units—particularly pre-PST lavas PSK-14 and PST-11, and post-PST magmatic enclaves in the Times and Moss porphyries and silicic lava SIT-1—appear to have the largest juvenile component, with relatively high ϵ_{Nd} and ϵ_{Hf} and low ⁸⁷Sr/⁸⁶Sr_i. Higher-SiO₂ units have lower ϵ_{Nd} and ϵ_{Hf} , and higher ⁸⁷Sr/⁸⁶Sr_i (Fig. 3).

The isotopic differences between the PST and all other SBMVC units except the Alcyone trachyte suggests that it, and perhaps the Alcyone as well, were petrogenetically distinct magmas. Notably, the intracaldera stocks and cross-cutting dikes have a similar range of compositions to the remainder of

pre- and post-PST units but do not overlap with the PST or the Alcyone sample

Zircon O and Hf isotopes

To our knowledge there are no published Hf isotope data for zircons or whole rocks representing the Proterozoic crust or young mafic rocks interpreted to be juvenile in the CREC region. Based on ϵ_{Nd} thought to represent the juvenile enriched lithospheric mantle (Fig. 3) and the terrestrial ϵ_{Nd} and ϵ_{Hf} array (Vervoort et al. 1999, 2011), we estimate that juvenile ϵ_{Hf} in the CREC is roughly -2 to -8. As discussed above, we estimate that Miocene ϵ_{Hf} in the Proterozoic Mojave crust is roughly in the range -17 to -33. An alternative estimate for Miocene ϵ_{Hf} of Paleoproterozoic rocks, based on the calculated ¹⁷⁶Hf/¹⁷⁷Hf of the six Paleoproterozoic zircons in our data set and typical ¹⁷⁶Lu/¹⁷⁷Hf of crustal rocks (~0.0125), falls toward the lower end of that range (-16.4 to -20.4). Based upon these estimates, our zircon ϵ_{Hf} data are consistent with whole-rock data in suggesting that magmatic sources comprised both ancient crustal and juvenile mantle-derived material (Fig. 4; Table 5), with the highest values of ~ -6 possibly representing growth from entirely juvenile magma and all others indicating highly variable amounts of hybridization.

Oxygen isotopic compositions of zircon are mostly >~5.6, somewhat heavier than expected for crystals grown from juvenile, mantle-derived magmas but mostly toward the lower end of the typical crustal zircon range. This further supports the inference that SBMVC magmas were hybrids that combined substantial proportions of juvenile mantle-derived and crustal components. The paucity of $\delta^{18}\text{O}$ values >+7 to +8‰ (Fig. 4; Supplemental Appendix 2¹) suggests limited input from metasedimentary sources (e.g., the abundant paragneisses of the Mojave terrane). A few relatively low $\delta^{18}\text{O}$ analyses ($\delta^{18}\text{O} = +4$ –5‰) from a silicic porphyry dike and Times porphyry zircons may reflect limited melting and assimilation of hydrothermally altered rock during the SBMVC’s post-PST magmatic stage (e.g., Bindeman and Valley 2001), but the dearth of these values suggests that, unlike the large-volume continental magmatic centers along the Yellowstone-Snake River Plain trend (Bindeman and Valley 2001; Watts et al. 2011; Drew et al. 2013), this process played a relatively minor role in the development and evolution of the PST and other SBMVC magmas.

Increasing average $\epsilon_{\text{Hf-zircon}}$ and decreasing $\delta^{18}\text{O}_{\text{zircon}}$ in post-

PST units is broadly consistent with whole-rock isotopic data that indicate increasing input of mantle-derived material into the SBMVC system after the PST eruption. This inference is supported by the relative abundance of post-PST zircons with enriched Mojave mantle-like zircon isotopic compositions (Fig. 5a).

Zircons from PST samples and the Alcyone trachyte have similar narrow ranges of relatively high $\delta^{18}\text{O}$ and low ϵ_{Hf} values, consistent with crystallization within an isotopically homogeneous magma body with a relatively large ancient crustal component. In contrast, zircons from most pre- and post-PST units and individual samples have wider isotopic ranges, lower average $\delta^{18}\text{O}$, and higher average ϵ_{Hf} (Figs. 4 and 5). These characteristics indicate crystallization from petrogenetically diverse magmas with greater contributions from juvenile sources than PST, or Alcyone trachyte. The large ranges in $\delta^{18}\text{O}$ and ϵ_{Hf} in zircon from many samples, in many cases beyond analytical uncertainty (see Supplemental Appendix 3¹), demonstrate isotopic disequilibrium. This indicates open-system processes whereby zircons crystallized in isotopically distinct melts prior to mingling and mixing (cf. McDowell et al. 2014).

Like the whole-rock data, zircon isotopic compositions reveal a petrogenetic distinction between the PST and intrusions. Moss porphyry zircon ages are within error of PST age (McDowell et al. 2014), but the two units are isotopically distinct: the Moss porphyry displays a greater range in $\delta^{18}\text{O}$ and ϵ_{Hf} than the PST and has a distinctly higher $\epsilon_{\text{Hf-WR}}$, $\epsilon_{\text{Nd-WR}}$, and average $\epsilon_{\text{Hf-zircon}}$; the Times porphyry and the dikes exhibit broadly similar averages and trends to those of the Moss porphyry. Thus, whereas effective isotopic homogenization of the PST magma body occurred prior to zircon saturation and crystallization (Frazier 2013), isotopic variability in zircons from the intrusions document mingling and mixing that is also clearly revealed in outcrop and thin section, for example by quenched mafic enclaves and resorbed and rimmed crystals (McDowell et al. 2014).

Integration of zircon and whole-rock Hf isotope data

Comparison and integration of zircon and whole-rock ϵ_{Hf} offers constraints on SBMVC magmatic evolution beyond what can be gleaned from either data set alone (Fig. 5b), providing insights into details of open-system processes.

In rocks that formed from magmas that evolved only by closed-system processes, zircon ϵ_{Hf} should be uniform and statistically identical to initial ϵ_{Hf} in their host rocks. Variation in zircon ϵ_{Hf} that exceeds variability that can be explained by analytical uncertainty for a uniform population suggests evolution involving open-system processes. As noted above, a majority of samples other than PST and Alcyone trachyte meet this criterion for identification of open-system processes. Furthermore, in most rocks globally of intermediate to silicic composition, a great majority of Hf resides in zircon; therefore, mean zircon ϵ_{Hf} should be very close to ϵ_{Hf} in host rocks. Where this is not the case, it reveals not only the influence of open-system processes, but also that a large fraction of whole-rock Hf is not represented by the analyzed zircon. Either the analyzed zircon population was highly non-representative (an important part of the range of compositions was missed), or much of the Hf in the rock is in other phases and has a distinctly different isotopic composition.

The range of zircon ϵ_{Hf} in a majority of samples spans the

whole-rock ϵ_{Hf} value and the mean zircon value is close to whole-rock (Fig. 5b). However, in four samples there is a strong apparent mismatch—two magmatic enclaves (one in the Moss porphyry [MPe1], one in the Times porphyry [SCM-27b]), a relatively mafic (trachyandesitic) zone within a composite feldspar porphyry dike (SCM-30), and a post-PST intermediate-composition lava (SIT-2)—in which most or all zircon ϵ_{Hf} values are either lower or higher than ϵ_{Hf} of their host whole rocks. In three cases zircon values are equal to or less than whole rock, and in the fourth they are equal to or greater than whole rock (Fig. 5b).

In the magmatic enclaves and feldspar porphyry dike, whole-rock ϵ_{Hf} exceeds calculated mean zircon ϵ_{Hf} by ~2 units; $\epsilon_{\text{Hf-WR}}$ of -8 to -10 indicates a larger juvenile component than $\epsilon_{\text{Hf-zircon}}$. For individual zircon analyses in these samples, ϵ_{Hf} is 0 to 5 units lower than whole-rock. However, the range of ϵ_{Hf} in magmatic enclave zircons is nearly identical to zircon ϵ_{Hf} ranges in their respective Times and Moss porphyry host rocks (Fig. 5b). We suggest that enclave zircons are likely xenocrysts entrained from the partially crystallized Times and Moss porphyry host magmas during the injection of more mafic, juvenile material. Similarly, the range of zircon ϵ_{Hf} in trachyandesitic sample SCM-30 matches the ϵ_{Hf} range in a more silicic section of the same composite dike (SCM-1b, trachytic), again indicating that the zircon bears the isotopic signature of its original host instead of the more juvenile magma into which it was incorporated. Assuming that our sample set is sufficiently statistically robust, any zircons that grew within the enclaves and dike melts were likely too small to extract via typical mechanical and gravimetric mineral separation methods.

In trachyte lava SIT-2, mean zircon ϵ_{Hf} exceeds whole-rock ϵ_{Hf} by ~3 units; the zircon has a more juvenile signature than its more crustal host. SIT-2 is characterized by large, 2–3 cm rounded feldspar glomerocrysts (some with reaction rims), phenocrysts (or xenocrysts) of biotite and sphene with reaction textures, and sparse clinopyroxene and feldspar microlites within a glassy matrix. We surmise that the differences in zircon and whole-rock ϵ_{Hf} reflect the injection of a more evolved magma into, and the partial resorption of, a less evolved feldspar-rich cumulate. We propose that the analyzed zircon was derived from the disaggregated cumulate, and therefore that its isotopic composition approaches that of the more primitive magma from which the cumulate crystallized; in contrast, the whole-rock composition of SIT-2 reflects that of the injected, more isotopically evolved, magma. The less radiogenic component of whole-rock Hf is probably in large part contained within the glassy matrix (melt).

Proposed evolution of the SBMVC

We propose the following reconstruction of the SBMVC's magmatic evolution based on whole-rock and zircon isotopic constraints in conjunction with field, elemental, and petrographic data (Fig. 6).

(1) ~19–18.8 Ma: Eruption of $\sim 10^3 \text{ km}^3$ of intermediate-composition magmas (trachytic and subordinate trachybasaltic and trachyandesitic lavas, Cook Canyon ignimbrite), all produced from a combination of juvenile, enrichedmantle-derived magma and Paleoproterozoic Mojave crustal material. Relative crustal contributions to pre-PST lavas were variable; Alcyone trachyte at the base of the pre-PST lava section records the greatest crustal contribution of analyzed pre-PST units (Figs. 3 and 4).

One pre-PST lava and a PST magmatic enclave provide isotopic evidence for input of magmas with dominantly sources prior to and during the PST episode.

(2) 18.8 Ma: Accumulation, homogenization, and eruption of the $>700 \text{ km}^3$ PST magma body. The narrow, relatively crust-rich whole-rock and zircon isotopic signatures in rhyolitic and trachytic PST (Figs. 3, 4, and 5) distinguish PST from all other analyzed units in the SBMVC except for the early Alcyone trachyte lava. The uniformity of zircon isotopic compositions suggests that zircon growth postdated mixing.

(3) 18.8–17 Ma: Episodic eruption and intrusion of relatively small volume, elementally and isotopically diverse magmas. Like their magmatic predecessors, post-PST magmas were generated from a combination of enriched mantle- and Paleoproterozoic crust-derived sources. However, they were more isotopically diverse and in general richer in the juvenile component. Intrasample variability in zircon isotopic composition, along with field and petrographic relations, demonstrates open-system processes and suggests that magma recharge periodically reinvigorated the volcanic center, locally disaggregating and assimilating resident crystal mushes or previously crystallized material.

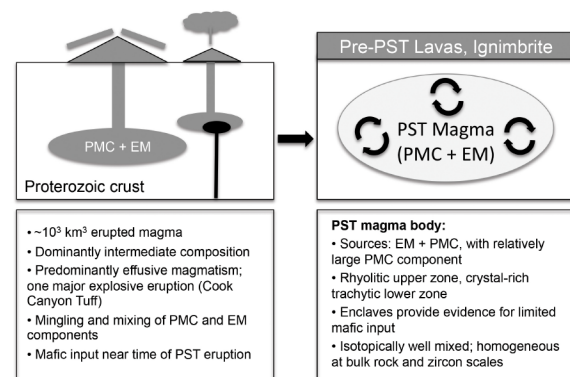
IMPLICATIONS

(1) Elemental and isotopic data for the PST and intracaldera plutons indicate that they are petrogenetically distinct: the caldera intrusions are more isotopically heterogeneous and record more juvenile input. Plausibly, the plutons may represent mush from the remains of the base of the PST chamber, rejuvenated and contaminated by more juvenile magma, but the data yield no isotopic evidence for a *direct* petrogenetic connection between the intracaldera plutons and the phenocryst-rich trachyte that has been interpreted as erupted PST mush.

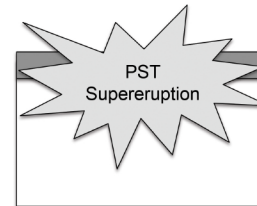
These findings are in this regard consistent with those from some other Cenozoic, large-eruption producing volcanic centers (such as Questa caldera in the Southern Rocky Mountain volcanic field; see Tappa et al. 2011) where intracaldera plutons are isotopically and temporally distinct from high-volume erupted material. Either the high-volume eruptions evacuated essentially all magma from the chamber, or any remaining material was subject to post-eruption modification, as suggested here.

(2) Previous studies (e.g., Tappa et al. 2011; Lipman 2007) have proposed that ignimbrite-producing felsic volcanic centers exhibit characteristic waxing and waning stages correlating with pre- and post-ignimbrite magmatism, respectively. Other studies (e.g., Annen et al. 2015) also document pre-supereruption thermal priming of the crust and post-supereruption diminished magmatic flux. The SBMVC appears to reflect a similar process. Mineral and whole rock isotopic data from the SBMVC reveal that although all SBMVC rocks formed via hybridization between regional enriched mantle magmas and Proterozoic Mojave crust, the supereruptive PST magma body incorporated a larger crustal component and experienced far more thorough hybridization than its magmatic predecessors or successors. This may suggest an increasing thermal flux prior to the PST eruption (consistent with thermal data reported in McDowell et al. 2014 for this system), transferred advectively from the mantle by mafic magmas and leading to more extensive crustal melting during the “waxing” phase of the SBMVC’s history, and the consequent formation a

1. Pre-PST Magmatism (19 – 18.8 Ma):

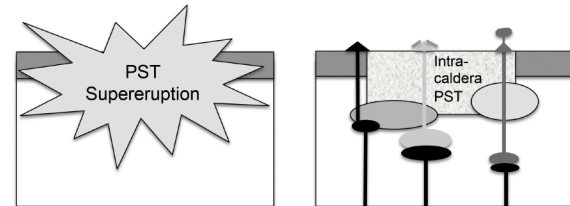


2. PST Supereruption (18.8 Ma):



- $>700 \text{ km}^3$ D.R.E. erupted
- Areal extent $>32,000 \text{ km}^2$
- Only supereruption within the CREC
- Dominated by high-silica rhyolite, lesser low-silica rhyolite and phenocryst-rich trachyte

3. Post-PST Magmatism (18.8 – 17 Ma):



- Periodic eruption, intrusion, crystallization of geochemically diverse, small-volume magmas
- Intracaldera intrusions: petrogenetically and genetically distinct from PST
- Sources: EM + PMC, with increasing EM contribution through time

FIGURE 6. Cartoon depicting the magmatic evolution of the SBMVC as indicated by elemental, isotopic, and field data. PMC = Proterozoic Mojave crust component; EM = enriched Mojave lithospheric mantle component.

much larger, hotter, more vigorously convecting magma body.

Subsequent diminished mantle flux resulted in abrupt post-PST waning of magmatism. Post-PST volcanic rocks and intrusions have more primitive whole-rock and zircon isotopic compositions than the PST; in the waning stages of magmatic flux within the SBMVC, these isotopic compositions become more primitive through time, indicating a relative increase in the proportion of mantle input to the regional magmatic system.

Increasing mantle fraction in the small-volume magmas was probably a consequence of one or both of two factors: (1) massive partial melting in the subjacent crust rendered it more refractory after the PST eruption, and hence the crust contributed a greatly reduced mass to ascending post-PST mantle-derived magmas; and/or (2) diminished mantle magma flux after the PST eruption resulted in cooling and greatly reduced melting in the crust, such that the modest amounts of magma that reached the upper crust had incorporated smaller crustal components.

ACKNOWLEDGMENTS

We thank Marsha Lidzbarski for her expertise and assistance in collecting the zircon data presented here, and Charles Ferguson (Arizona Geological Survey) for sharing his extensive knowledge of the southern Black Mountains and of field volcanology in general, and for his assistance in collecting representative samples. Jeff Vervoort, Charles Knaack, Diane Wilford, and Scott Boroughs kindly lent their expertise and facilitated our work at the Washington State Radiogenic Isotope and Geochronology Laboratory. Reviewers Lang Farmer and Peter Lipman and Associate Editor Calvin Barnes provided thorough, careful, constructive comments

that were very helpful in revising and improving the manuscript. This research was supported by collaborative NSF grants EAR-0409876 and 0911726 (Vanderbilt) and EAR-0409882 and 0911728 (San Jose State).

REFERENCES CITED

- Allen, C.M., Wooden, J.L., Howard, K.A., Foster, D.A., and Tosdal, R.M. (1995) Sources of the Early Cretaceous plutons in the Turtle and West Riverside mountains, California; anomalous Cordilleran interior intrusions. *Journal of Petrology*, 36, 1675–1700.
- Annen, C., Blundy, J.D., Leuthold, J., and Sparks, S.J. (2015) Construction and evolution of igneous bodies: Towards an integrated perspective of crustal magmatism. *Lithos*, 230, 206–221.
- Bachl, C.A., Miller, C.F., Miller, J.S., and Faulds, J.E. (2001) Construction of a pluton: Evidence from an exposed cross-section of the Searchlight pluton, Eldorado Mountains, Nevada. *GSA Bulletin*, 113, 1213–1228.
- Bachmann, O., and Bergantz, G.W. (2004) On the origin of crystal-poor rhyolites: extracted from batholithic crystal mushes. *Journal of Petrology*, 45, 1565–1582.
- (2008) The magma reservoirs that feed supereruptions. *Elements*, 4, 17–21.
- Bachmann, O., Miller, C.F., and De Silva, S.L. (2007) The volcanic–plutonic connection as a stage for understanding crustal magmatism. *Journal of Volcanology and Geothermal Research*, 167, 1–23.
- Baertschi, P. (1976) Absolute $\delta^{18}\text{O}$ content of standard mean ocean water. *Earth and Planetary Science Letters*, 31, 341–344.
- Bennett, V.C., and DePaolo, D.J. (1987) Proterozoic crustal history of the western United States as determined by neodymium isotopic mapping. *Geological Society of America Bulletin*, 99, 674–685.
- Bindeman, I.N., and Valley, J.W. (2001) Low- $\delta^{18}\text{O}$ rhyolites from Yellowstone: magmatic evolution based on analyses of zircons and individual phenocrysts. *Journal of Petrology*, 42, 1491–1517.
- Bindeman, I.N., Watts, K.E., Schmitt, A.K., Morgan, L.A., and Shanks, P.W. (2007) Voluminous low $\delta^{18}\text{O}$ magmas in the late Miocene Heise volcanic field, Idaho: Implications for the fate of Yellowstone hotspot calderas. *Geology*, 35, 1019–1022.
- Blichert-Toft, J. (2008) The Hf isotopic composition of zircon reference material 91500. *Chemical Geology*, 253, 252–257.
- Blichert-Toft, J., Chauvel, C., and Albarède, F. (1997) Separation of Hf and Lu for high-precision isotope analysis of rock samples by magnetic sector-multiple collector ICP-MS. *Contributions to Mineralogy and Petrology*, 127, 248–260.
- Bouvier, A., Vervoort, J.D., and Patchett, P.J. (2008) The Lu-Hf and Sm-Nd isotopic composition of CHUR: constraints from unequilibrated chondrites and implications for the bulk composition of terrestrial planets. *Earth and Planetary Science Letters*, 273, 48–57.
- Buesch, D.C. (1991) Changes in depositional environments resulting from emplacement of a large-volume ignimbrite. *Special Publication—Society of Economic Paleontologists and Mineralogists*, 45, 139–153.
- Buesch, D.C., and Valentine, G.A. (1986) Peach Springs Tuff and volcanic stratigraphy of the southern Cerbat Mountains, Kingman, Arizona. In J.E. Nielson, and A.F. Glazner, Eds., *Cenozoic Stratigraphy, Structure and Mineralization in the Mojave Desert*, p. 7–14. California State University, Los Angeles.
- Daley, E.E., and DePaolo, D.J. (1992) Isotopic evidence for lithospheric thinning during extension; southeastern Great Basin. *Geology*, 20, 104–108.
- DePaolo, D.J., and Daley, E.E. (2000) Neodymium isotopes in basalts of the southwest basin and range and lithospheric thinning during continental extension. *Chemical Geology*, 169, 157–185.
- DeWitt, E., Thorson, J.P., and Smith, R.C. (1986) Geology and gold deposits of the Oatman District, northwestern Arizona. *U.S. Geological Survey Bulletin*, 1857-1, II-128.
- Drew, D.L., Bindeman, I.N., Watts, K.E., Schmitt, A.K., Fu, B., and McCurry, M. (2013) Crustal-scale recycling in caldera complexes and rift zones along the Yellowstone hotspot track: O and Hf isotopic evidence in diverse zircons from voluminous rhyolites of the Picabo volcanic field, Idaho. *Earth and Planetary Science Letters*, 381, 63–77.
- Erickson, S.M., Miller, J.S., Miller, C.F., Harper, B.E., and Aggarwal, J.K. (2004) Isotopic constraints on the evolution of felsic magma in the Aztec Wash pluton, Eldorado Mountains, Nevada. *Geological Society of America Abstracts with Programs*, 36, 8.
- Falkner, C.M., Miller, C.F., Wooden, J.L., and Heizler, M.T. (1995) Petrogenesis and tectonic significance of the calc-alkaline, bimodal Aztec Wash pluton, Eldorado Mountains, Colorado River extensional corridor. *Journal of Geophysical Research*, 100(B7), 10453–10476.
- Farmer, G.L., Perry, F.V., Semken, S., Crowe, B., Curtis, D., and DePaolo, D.J. (1989) Isotopic evidence of the structure and origin of subcontinental lithospheric mantle in southern Nevada. *Journal of Geophysical Research*, 94, 7885–7898.
- Faulds, J.E., Geissman, J.W., and Mawer, C.K. (1990) Structural development of a major extensional accommodation zone in the Basin and Range Province, northwestern Arizona and southern Nevada; Implications for kinematic models of continental extension. *Geological Society of America Memoirs*, 176, 37–76.
- Faulds, J.E., Feuerbach, D.L., Reagan, M.K., Metcalf, R.V., Gans, P., and Walker, J.D. (1995) The Mount Perkins block, northwestern Arizona: An exposed cross-section of an evolving, preextensional to synextensional magmatic system. *Journal of Geophysical Research*, 100, 15249–15266.
- Faulds, J.E., Smith, E.I., and Gans, P. (1999) Spatial and temporal patterns of magmatism and extension in the northern Colorado River extensional corridor, Nevada and Arizona: A preliminary report. In *Cenozoic geology of the northern Colorado River extensional corridor, Nevada and Arizona: Economic implications of extensional segmentation structures*: Nevada Petroleum Society, Field Trip Guide, 171–183.
- Faulds, J.E., Feuerbach, D.L., Miller, C.F., and Smith, E.I. (2001) Cenozoic evolution of the northern Colorado River extensional corridor, southern Nevada and northwest Arizona. In M.C. Erskine, J.E. Faulds, J.M. Bartley, and P.D. Rowley, Eds., *The Geologic Transition, High Plateaus to Great Basin—A symposium and field guide: The Makin volume*: Utah Geological Association Publication 30, Pacific Section American Association of Petroleum Geologists Publication GB78, 239–271.
- Ferguson, C.A., McIntosh, W.C., and Miller, C.F. (2013) Silver Creek caldera—The tectonically dismembered source of the Peach Spring Tuff. *Geology*, 41, 3–6.
- Feuerbach, D.L., Smith, E.I., Walker, J.D., and Tangeman, J.A. (1993) The role of the mantle during crustal extension: Constraints from geochemistry of volcanic rocks in the Lake Mead area, Nevada and Arizona. *Geological Society of America Bulletin*, 105, 1561–1575.
- Feuerbach, D.L., Reagan, M.K., Faulds, J.E., and Walker, J.D. (1998) Lead isotopic evidence for synextensional lithospheric ductile flow in the Colorado River extensional corridor, western United States. *Journal of Geophysical Research: Solid Earth* (1978–2012), 103(B2), 2515–2528.
- Fisher, C.M., Vervoort, J.D., and DuFrane, S.A. (2014a) Accurate Hf isotope determinations of complex zircons using the “laser ablation split stream” method. *Geochemistry, Geophysics, Geosystems*, 15, 121–139.
- Fisher, C.M., Vervoort, J.D., and Hanchar, J.M. (2014b) Guidelines for reporting zircon Hf isotopic data by LA-MC-ICPMS and potential pitfalls in the interpretation of these data. *Chemical Geology*, 363, 125–133.
- Frazier, W.O. (2013) Petrochemical constraints on generation of the Peach Spring Tuff supereruption magma, Arizona, Nevada, California. Masters thesis, Vanderbilt University.
- Galer, S.J.G., and Abouchami, W. (1998) Practical application of lead triple spiking for correction of instrumental mass discrimination. *Mineralogical Magazine of America*, 62, 491–492.
- Gaschnig, R.M., Vervoort, J.D., Lewis, R.S., and Tikoff, B. (2011) Isotopic evolution of the Idaho batholith and Challis intrusive province, northern US Cordillera. *Journal of Petrology*, 52, 2397–2429.
- Gerber, M.E., Miller, C.F., and Wooden, J.L. (1995) Plutonism at the eastern edge of the Cordilleran Jurassic magmatic belt, Mojave Desert, California. In D.M. Miller and C. Busby, Eds., *Jurassic Magmatism and Tectonism in the Cordillera*, Geological Society of America Special Paper, 299, 351–374.
- Glazner, A.F., Nielson, J.E., Howard, K.E., and Miller, D.M. (1986) Correlation of the Peach Springs Tuff, a large-volume Miocene ignimbrite sheet in California and Arizona. *Geology*, 14, 840–843.
- Glazner, A.F., Coleman, D.S., and Bartley, J.M. (2008) The tenuous connection between high-silica rhyolites and granodiorite plutons. *Geology*, 36, 183–186.
- Hawkesworth, C.J., and Kemp, A.I.S. (2006) Using hafnium and oxygen isotopes in zircons to unravel the record of crustal evolution. *Chemical Geology*, 226, 144–162.
- Kapp, J.L., Miller, C.F., and Miller, J.S. (2002) Ireneba pluton, Eldorado Mountains, Nevada: Late, deep-source, peraluminous magmatism in the Cordilleran Interior. *Journal of Geology*, 110, 649–669.
- Kemp, A.I.S., Hawkesworth, C.J., Paterson, B.A., and Kinny, P.D. (2006) Episodic growth of the Gondwana supercontinent from hafnium and oxygen isotopes in zircon. *Nature*, 439, 580–583.
- Kemp, A.I.S., Hawkesworth, C.J., Foster, G.L., Paterson, B.A., Woodhead, J.D., Herdt, J.M., Gray, C.M., and Whitehouse, M.J. (2007) Magmatic and crustal differentiation history of granitic rocks from Hf-O isotopes in zircon. *Science*, 315, 980–983.
- Kemp, A.I.S., Wilde, S.A., Hawkesworth, C.J., Coath, C.D., Nemchin, A., Pidgeon, R.T., Vervoort, J.D., and DuFrane, S.A. (2010) Hadean crustal evolution revisited: new constraints from Pb–Hf isotope systematics of the Jack Hills zircons. *Earth and Planetary Science Letters*, 296, 45–56.
- Lang, N. (2001) Evolution of the Secret Pass Canyon volcanic center, Colorado River Extensional Corridor, northwest Arizona. M.S. thesis, p. 114 p. Vanderbilt University, Nashville, Tennessee.
- Lang, N.P., Walker, B.J., Clairborne, L.L., Miller, C.F., Hazlett, R.W., and Heizler, M.T. (2008) The Spirit Mountain batholith and Secret Pass Canyon volcanic center: A cross-sectional view of the magmatic architecture of the uppermost crust of an extensional terrain, Colorado River, Nevada–Arizona: Geological Society of America Field Guide, 11, 187–214, doi:10.1130/2008.fl011(09).
- Le Bas, M.J., Le Maitre, R.W., Streckeisen, A., and Zanettin, B.A. (1986) Chemical classification of volcanic rocks based on the total alkali-silica diagram. *Journal of Petrology*, 27, 745–750.
- Lidzbarski, M.I. (2014) U-Pb Geochronology of the Miocene Peach Spring Tuff Supereruption And Precursor Cook Canyon Tuff, Western Arizona, USA.

- Master's thesis, Paper 4502. http://scholarworks.sjsu.edu/etd_theses/4502.
- Lidzbarski, M., Mundil, R., Miller, J.S., and Vasquez, J.A. (2012) Comparing pre- and post-chemical abrasion ages for Miocene Peach Springs Tuff zircon from ID-TIMS and SIMS analyses. AGU Fall Meeting, December 2012.
- Lipman, P.W. (1984) The roots of ash flow calderas in western North America: Windows into the tops of granitic batholiths. *Journal of Geophysical Research: Solid Earth*, 89(B10), 8801–8841.
- (2007) Incremental assembly and prolonged consolidation of Cordilleran magma chambers: Evidence from the Southern Rocky Mountain volcanic field. *Geosphere*, 3, 42–70.
- McDowell, S.M., Miller, C.F., Ferguson, C.A., Fisher, C., Frazier, W.O., Miller, J.S., Mundil, R., Overton, S., and Vervoort, J. (2012) Geochemical insights into the evolution of a supereruptive volcanic center: magmatic precursors and successors of the Miocene Peach Spring Tuff, southern Black Mountains, western AZ. Geological Society of America Abstracts with Programs, 44, 320.
- McDowell, S.M., Miller, C.F., Mundil, R., Ferguson, C.A., and Wooden, J.L. (2014) Zircon evidence for a ~200 ky supereruption-related thermal flare-up in the Miocene southern Black Mountains, western Arizona, USA. *Contributions to Mineralogy and Petrology*, 168, 1–21.
- Metcalf, R.V. (2004) Volcanic-plutonic links, plutons as magma chambers and crust–mantle interaction: a lithospheric scale view of magma systems. *Transactions of the Royal Society of Edinburgh: Earth Sciences*, 95, 357–374.
- Metcalf, R.V., Smith, E.I., Walker, J.D., Reed, R.C., and Gonzales, D.A. (1995) Isotopic disequilibrium among commingled hybrid magmas: evidence for a two-stage magma mixing-commingling process in the Mt. Perkins pluton, Arizona. *Journal of Geology*, 103, 509–527.
- Miller, C.F., and Miller, J.S. (2002) Contrasting stratified plutons exposed in tilt blocks, Eldorado Mountains, Colorado River Rift, NV, USA. *Lithos*, 61, 209–224.
- Miller, C.F., and Wooden, J.L. (1994) Anatexis, hybridization and the modification of ancient crust: Mesozoic plutonism in the Old Woman Mountains area, California. *Lithos*, 32, 111–133.
- Miller, J.S., Glazner, A.F., Farmer, G.L., Suayah, I.B., and Keith, L.A. (2000) A Sr, Nd, and Pb isotopic study of mantle domains and crustal structure from Miocene volcanic rocks in the Mojave Desert, California. *Geological Society of America Bulletin*, 112, 1264–1279.
- Mills, R.D., and Coleman, D.S. (2013) Temporal and chemical connections between plutons and ignimbrites from the Mount Princeton magmatic center. *Contributions to Mineralogy and Petrology*, 165, 961–980.
- Morel, M.L.A., Nebel, O., Nebel-Jacobsen, Y.J., Miller, J.S., and Vroon, P.Z. (2008) Hafnium isotope characterization of the GJ-1 zircon reference material by solution and laser-ablation MC-ICPMS. *Chemical Geology*, 255, 231–235.
- Murphy, R.T. (2004) Tectono-magmatic interaction and extensional folding in the Union Pass area, northern Colorado River extensional corridor, northwest Arizona. M.S. thesis, University of Nevada, Reno, 150 p.
- Murphy, R.T., and Faulds, J.E. (2003) Interactions between Tertiary magmatism and extension in the Colorado River Extensional Corridor, Union Pass area, northwestern Arizona. Geological Society of America Abstracts with Programs, 35, 348.
- (2013) Preliminary Geologic Map of the North Half of the Union Pass Quadrangle, Mohave County, Arizona. Arizona Geological Survey Contributed Map, CM-13-A, 1 map sheet, map scale 1:24,000.
- Murphy, R.T., Faulds, J.E., and Hillmeyer, F.L. (2004) Evolution of Miocene extensional fault and fold systems and influence of magmatism in the northern Colorado River extensional corridor, Union Pass area, northwest Arizona. Geological Society of America Abstracts with Programs, 36, 21.
- Pamukcu, A.S., Carley, T.L., Gualda, G.A., Miller, C.F., and Ferguson, C.A. (2013) The evolution of the Peach Spring giant magma body: Evidence from accessory mineral textures and compositions, bulk pumice and glass geochemistry, and rhyolite-MELTS modeling. *Journal of Petrology*, 54, 1109–1148.
- Patchett, P.J., and Tatsumoto, M. (1981) A routine high-precision method for Lu-Hf isotope geochemistry and chronology. *Contributions to Mineralogy and Petrology*, 75, 263–267.
- Pearthree, P.A., Ferguson, C.A., Johnson, B.J., and Guynn, J. (2010) Geologic Map and Report for the Proposed State Route 95 Realignment Corridor, Mohave County, Arizona, v. 1: Arizona Geological Survey DGM-65, 5 sheets, 1:24,000 scale, 44 pp.
- Prytulak, J., Vervoort, J.D., Plank, T., and Yu, C. (2006) Astoria Fan sediments, DSDP site 174, Cascadia Basin: Hf-Nd-Pb constraints on provenance and outburst flooding. *Chemical Geology*, 233, 276–292.
- Ransome, F.L. (1923) Geology of the Oatman gold district, Arizona: U.S. Geological Survey Bulletin, 743, 58 p.
- Renne, P.R., Mundil, R., Balco, G., Min, K., and Ludwig, K.R. (2010) Joint determination of ^{40}K decay constants and $^{40}\text{Ar}^*/^{40}\text{K}$ for the Fish Canyon sanidine standard, and improved accuracy for $^{40}\text{Ar}/^{39}\text{Ar}$ geochronology. *Geochimica et Cosmochimica Acta*, 74, 5349–5367.
- Renne, P.R., Balco, G., Ludwig, K.R., Mundil, R., and Min, K. (2011) Response to the comment by WH Schwartz et al. on "Joint determination of ^{40}K decay constants and $^{40}\text{Ar}^*/^{40}\text{K}$ for the Fish Canyon sanidine standard, and improved accuracy for $^{40}\text{Ar}/^{39}\text{Ar}$ geochronology" by PR Renne et al. (2010) *Geochimica et Cosmochimica Acta*, 75, 5097–5100.
- Schoene, B., Crowley, J.L., Condon, D.J., Schmitz, M.D., and Bowring, S.A. (2006) Reassessing the uranium decay constants for geochronology using ID-TIMS U-Pb data. *Geochimica et Cosmochimica Acta*, 70, 426–445.
- Tappa, M.J., Coleman, D.S., Mills, R.D., and Samperton, K.M. (2011) The plutonic record of a silicic ignimbrite from the Latir volcanic field, New Mexico. *Geochemistry, Geophysics, Geosystems*, 12, Q10011.
- Thorson, J.P. (1971) Igneous petrology of the Oatman district, Mohave County, Arizona. Ph.D. thesis, University of California–Santa Barbara, 189 p.
- Trail, D., Mojzsis, S.J., Harrison, T.M., Schmitt, A.K., Watson, E.B., and Young, E.D. (2007) Constraints on Hadean zircon protoliths from oxygen isotopes, Ti-thermometry, and rare earth elements. *Geochemistry, Geophysics, Geosystems*, 8(6).
- Valley, J.W., Lackey, J.S., Cavosie, A.J., Clechenko, C.C., Spicuzza, M.J., Basei, M.A.S., Bindeman, I.N., Ferreira, V.P., Sial, A.N., King, E.M., and others. (2005) 4.4 billion years of crustal maturation: oxygen isotope ratios of magmatic zircon. *Contributions to Mineralogy and Petrology*, 150, 561–580.
- Varga, R.J., Faulds, J.E., Snee, L.W., Harlan, S.S., and Bettison-Varga, L. (2004) Miocene extension and extensional folding in an anticlinal segment of the Black Mountains accommodation zone, Colorado River extensional corridor, southwestern United States. *Tectonics*, 23, TC1019.
- Vervoort, J.D., Patchett, P.J., Blachert-Toft, J., and Albarede, F. (1999) Relationships between Lu-Hf and Sm-Nd isotopic systems in the global sedimentary system. *Earth and Planetary Science Letters*, 168, 79–99.
- Vervoort, J.D., Plank, T., and Prytulak, J. (2011) The Hf-Nd isotopic composition of marine sediments. *Geochimica et Cosmochimica Acta*, 75, 5903–5926.
- Walker, B.A. Jr., Miller, C.F., Lowery Claiborne, L., Wooden, J.L., and Miller, J.S. (2007) Geology and geochronology of the Spirit Mountain batholith, southern Nevada: implications for timescales and physical processes of batholith construction. *Journal of Volcanology and Geothermal Research*, 167, 239–262.
- Watts, K.E., Bindeman, I.N., and Schmitt, A.K. (2011) Large-volume rhyolite genesis in caldera complexes of the Snake River Plain: Insights from the Kilgore Tuff of the Heise Volcanic Field, Idaho, with comparison to Yellowstone and Bruneau–Jarbidge Rhyolites. *Journal of Petrology*, 52, 857–890.
- (2012) Crystal scale anatomy of a dying supervolcano: an isotope and geochronology study of individual phenocrysts from voluminous rhyolites of the Yellowstone caldera. *Contributions to Mineralogy and Petrology*, 164, 45–67.
- Wooden, J.L., and Miller, D.M. (1990) Chronologic and isotopic framework for early Proterozoic crustal evolution in the eastern Mojave desert region, SE California. *Journal of Geophysical Research*, 95(B12), 20,133–20,146.
- Wooden, J.L., Stacey, J.S., Howard, K.A., Doe, B.R., and Miller, D.M. (1988) Pb isotopic evidence for the formation of Proterozoic crust in the southwestern United States. In W.G. Ernst, Ed., *Metamorphism and Crustal Evolution in the Western United States*, p. 68–86. Prentice Hall, Englewood Cliffs, New Jersey.
- Woodhead, J.D., and Hergt, J.M. (2005) A preliminary appraisal of seven natural zircon reference materials for in situ Hf isotope determination. *Geostandards and Geoanalytical Research*, 29, 183–195.
- Young, R.A., and Brennan, W.J. (1974) Peach Springs Tuff: Its bearing on structural evolution of the Colorado Plateau and development of Cenozoic drainage in Mohave County, Arizona. *GSA Bulletin*, 85, 83–90.
- Zimmerer, M.J., and McIntosh, W.C. (2012a) An investigation of caldera-forming magma chambers using the timing of ignimbrite eruptions and pluton emplacement at the Mt. Aetna caldera complex. *Journal of Volcanology and Geothermal Research*, 245–246, 128–148.
- (2012b) The geochronology of volcanic and plutonic rocks at the Questa caldera: Constraints on the origin of caldera-related silicic magmas. *Geological Society of America Bulletin*, 124, 1394–1408.

MANUSCRIPT RECEIVED JULY 14, 2014

MANUSCRIPT ACCEPTED OCTOBER 2, 2015

MANUSCRIPT HANDLED BY CALVIN BARNES